Ultrasound Detection with Silicon Microring Resonators

Sarika Madhvapathy
Vladimir Stojanovic, Ed.
Ming C. Wu, Ed.

Electrical Engineering and Computer Sciences
University of California, Berkeley

Technical Report No. UCB/EECS-2021-123
http://www2.eecs.berkeley.edu/Pubs/TechRpts/2021/EECS-2021-123.html

May 14, 2021

Ultrasound Detection with Silicon Microring Resonators

by

Sarika Madhvapathy

A thesis submitted in partial satisfaction of the

requirements for the degree of

Master of Science

in

Electrical Engineering and Computer Sciences

in the

Graduate Division

of the

University of California, Berkeley

Committee in charge:

Professor Vladimir Stojanovic, Chair
Professor Ming Wu

Spring 2021

Ultrasound Detection with Silicon Microring Resonators

by Sarika Madhvapathy

Research Project

Submitted to the Department of Electrical Engineering and Computer Sciences, University of California at Berkeley, in partial satisfaction of the requirements for the degree of **Master of Science, Plan II**.

Approval for the Report and Comprehensive Examination:

Committee:

[illegible]

Professor Vladimir Stojanovic
Research Advisor

5/14/21

(Date)

* * * * * * *

[illegible]

Professor Ming Wu
Second Reader

5/10/2021

(Date)

Ultrasound Detection with Silicon Microring Resonators

Abstract

Ultrasound Detection with Silicon Microring Resonators

by

Sarika Madhvapathy

Master of Science in Electrical Engineering and Computer Sciences

University of California, Berkeley

Professor Vladimir Stojanovic, Chair

Ultrasound imaging systems are essential for breast tumor detection, stenting operations, and other endoscopic imaging applications. A beamforming array of silicon microring resonators (MRRs) is a promising solution for ultrasound imaging, as MRRs have been shown to have high sensitivity and high bandwidth. The power hungry circuitry of the analog front-end can be easily remoted outside of the body through a probe tube due to the small diameter of optical fibers. Using a comb laser, it is possible to interrogate an entire row with just one input. This helps reduce the probe tube size even further, as each input for a row requires a single optical fiber. With small diameters and remoted analog front end, the ring sensors can be compacted into a much smaller area, thus enabling higher bandwidth and higher resolution images. This technical report presents ultrasound receiver measurement results as well as photonic layout and analog designs for potential future generations of the project.

Contents

List of Figures

List of Tables

Listings

Acknowledgments

Thanks to Panagiotis Zarkos for all of his help and guidance, to Sidney Buchbinder for helping me debug all my BPG errors, to Professor Vladimir Stojanovic for advising me, to Christos Adamopoulos and the rest of the group, to the CITRIS Invention Lab for 3D-printing several water tanks for us, and to my friends and family for their support.

Chapter 1

Introduction

1.1 Project overview

Motivation

Ultrasound imaging systems are essential for breast tumor detection, stenting operations, and other endoscopic imaging applications. However, while they use established technology, commercial ultrasound imagers with piezoelectric micromachined ultrasound transducers (PMUTs) or capacitive micromachined ultrasound transducers (CMUTs) have several drawbacks:

- high probe form factor,
- high power consumption inside the body,
- large probe tube diameter,
- and limited bandwidth due to pitch constraints ($\lambda/2$ to avoid formation of grating lobes, where λ is the wavelength corresponding to the operating frequency).

In the past, sub-array beamforming [2] and element level digitization [5] have been proposed in order to address the difficulty of minimizing the number of interfacing cables for a large number of sensors in order to maintain an adequately small probe tube size.

Proposed solution

A silicon microring resonator (MRR) experiences pressure-induced modulation of its resonant frequency due to waveguide deformation, ring elongation, and the opto-elastic effect [7]. This resonant frequency modulation results in modulation of the output optical power, which can be converted to a voltage through a analog front end (AFE) consisting of a ring photodetector and a transimpedance amplifier (TIA). MRRs have also been shown to have high sensitivity [6] and high bandwidth.

Furthermore, the power hungry circuitry of each AFE can be easily remoted outside of the body through the probe tube in a dual-chip scheme, as the diameter of optical fibers is significantly smaller than that of the micro-coaxial cables used in PMUT-based ultrasound imaging systems.

Ring resonators behave like a notch filter with the notch located at the ring's resonant wavelength. Using a comb laser with comb teeth parked at the flanks of the resonant wavelengths for each ring in a row, it is possible to interrogate an entire row with just one input. This helps reduce the probe tube size even further, as only a single optical fiber is required as input for all of the rows.

With diameters of approx. 10 μm and remoted analog front end, the ring sensors can be compacted into a much smaller area, thus enabling higher bandwidth ($\lambda/2$ pitch) and higher resolution images. For all of these reasons, implementing a beamforming array of MRRs is a promising solution for ultrasound imaging.

1.2 Report overview

The purpose of this technical report is to provide results for the current generation of this project as well as potential ideas for future iterations. This report surveys three different aspects of this project:

1. measurement results,
2. photonic layout with Berkeley Photonic Generator (BPG),
3. and a potential redesign of the analog front end (AFE).

Chapter 2

Optical Ultrasound Receiver Measurements

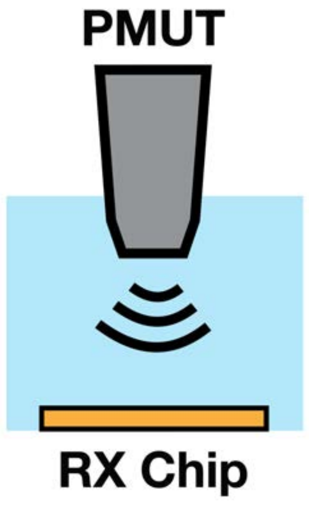

Figure 2.1: Immersion PMUT impinging pressure through water onto the receiver chip.

This chapter presents the measurement setup and measurement results for the MRR ultrasound receivers using both the on-chip analog frontend as well as an external photodiode with transimpedance amplifier (PD-TIA) for bandwidth measurements. It also displays the measured frequency responses of commercial PMUT immersion transducers used to impinge pressure upon the MRR receivers (as in Figure 2.1) using a commercial hydrophone with known sensitivity.

2.1 Experimental setup

Calibration setup

The pressure applied onto the chip by the PMUT is not known a priori, thus requiring a measurement setup to characterize the pressure exerted by the transducer using a commercial hydrophone with known sensitivity. This enables an accurate receiver sensitivity estimate, as the sensitivity for a ring is a function of the applied pressure.

Figure 2.2 details the measurement setup for the hydrophone measurements. A hole with diameter slightly smaller than the base of a standard-size immersion ultrasonic transducer is drilled at the bottom of a sealed resin water tank. An immersion transducer inside the tank is screwed into a UHF-to-BNC connector on the outside of the tank through the hole, thus sealing the bottom of the tank. The tank is propped up on either side of the hole to make room at the bottom of the tank for the UHF-to-BNC connector and its attached BNC cable.

An Onda HGL-series hydrophone is positioned above the transducer using an external adjustable Thorlabs stage with the tip facing the transducer. The tank is filled with water such that both the transducer and the hydrophone are fully immersed.

The hydrophone output is fed into an Onda pre-amplifier with 20 dB voltage gain before being read by the oscilloscope. An arbitrary wave generator (AWG) is used to excite the ultrasound transducer through the BNC cable at the bottom of the tank. One signal from the AWG's differential output is used to trigger the oscilloscope, while the other is used to excite the transducer. The peak-to-peak voltage output of the pre-amplifier is measured on the oscilloscope and recorded manually on a PC.

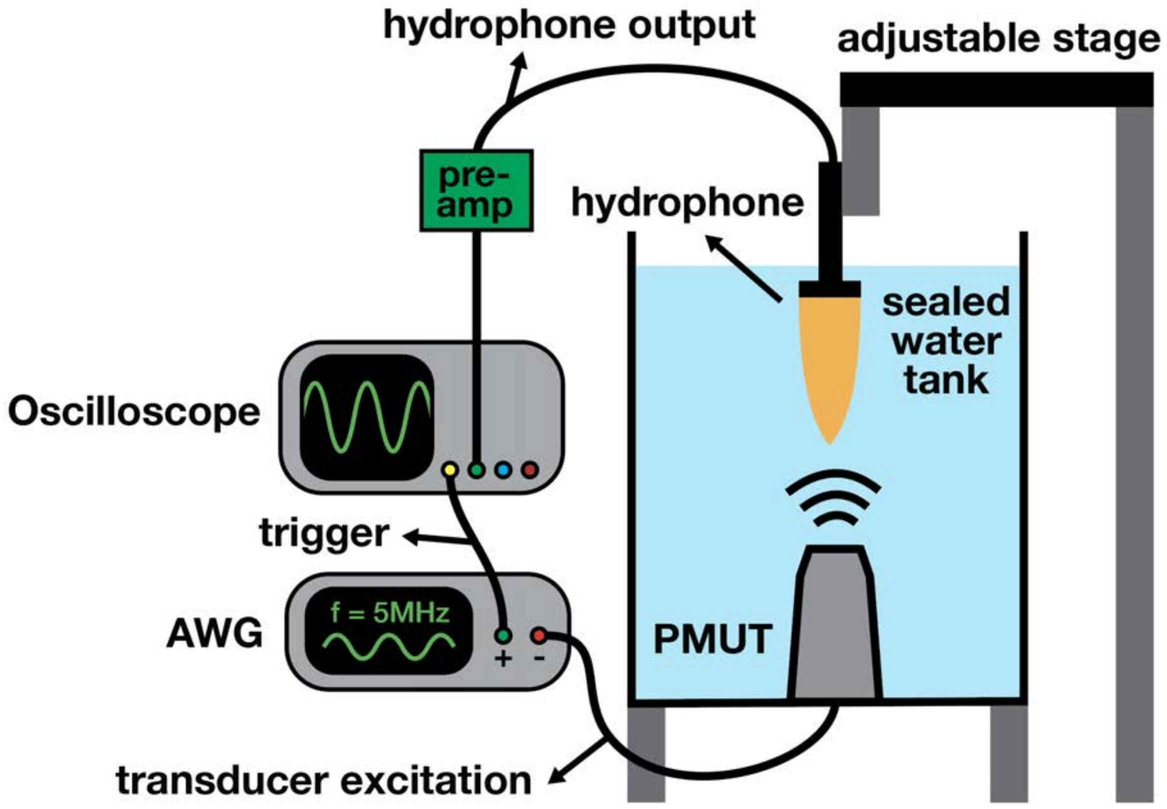

Figure 2.2: Hydrophone measurement setup.

Breakout board design and electrical testing setup

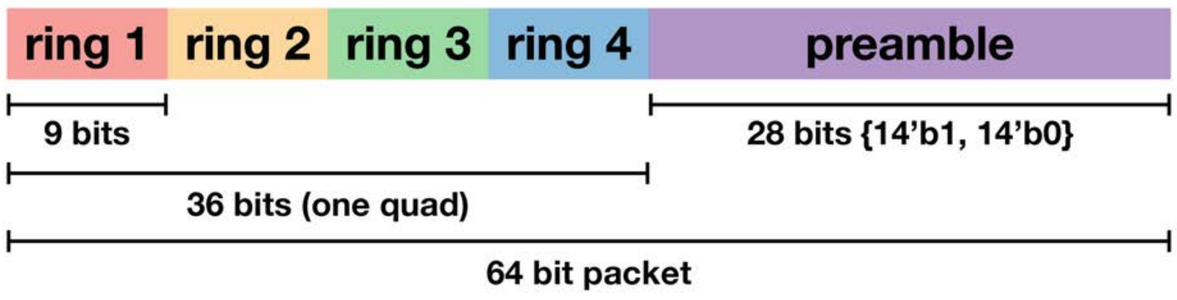

Figure 2.3: One 64-bit data packet, which contains the ADC output for a receiver quad.

The MRRs on the chip itself can both sense and receive, as each ring has dedicated analog frontend (AFE) circuitry to receive the modulated signal.

The AFE for a ring is routed to a successive-approximation (SAR) analog-to-digital converter (ADC) that converts the analog signal to a 9-bit digital signal. For each quad of sensing rings, the ADC outputs are concatenated and appended to a 28-bit preamble, as shown in Figure 2.3. The 64-bit packets for each quad are then serialized with a 64-to-1 serializer and output through the hostboard's FPGA mezzanine card (FMC) connector, with the intent of receiving these packets through the GTX/GTH transceivers on a Xilinx field-programmable gate array (FPGA) board and processing the data in real time.

To circumvent delays in verifying the Xilinx FPGA boards' transceiver functionality, it is possible to save the waveforms to an oscilloscope and process the data in post. This required the design of a custom SubMiniature version A (SMA) breakout board to read out the serial data, as most existing FMC breakout boards have the incorrect FMC connector type since they are designed to connect to an FPGA board rather than a daughterboard.

The PCB pictured in Figure 2.4 was designed with Altium Designer. The 2-layer board has 16 differential outputs (for a total of 32 SMA connectors) and one differential clock input (2 more SMA connectors) that is used to clock the on-chip ADCs. 16 SMA connectors are surface mount edge connectors and 18 are through-hole top connectors. The routing utilizes 50 Ohm coplanar ground waveguides; the ground planes on the top and bottom are stitched together using a via array. Each differential pair was designed to have matched lengths.

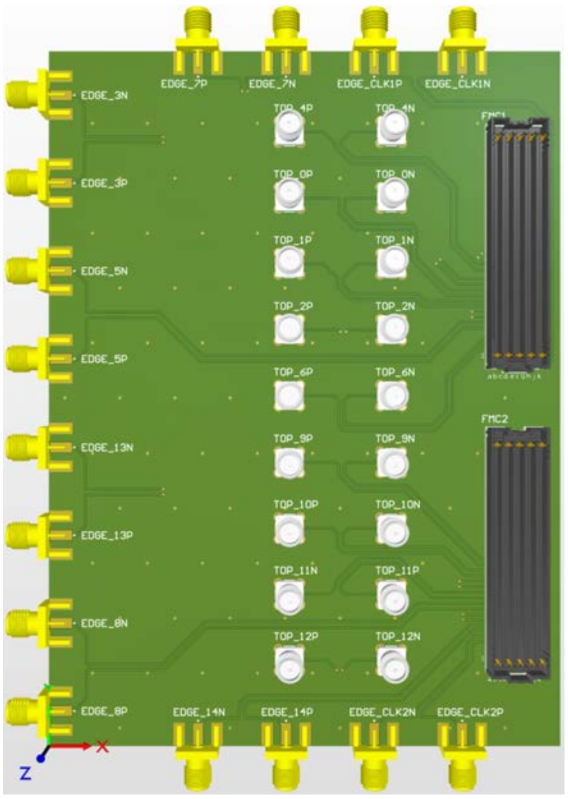

(a) Three-dimensional rendering of front of breakout board.

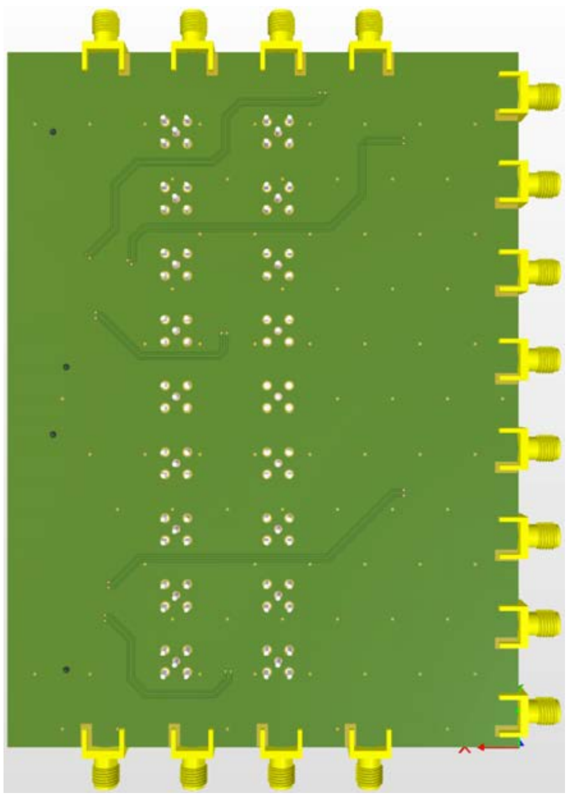

(b) Three-dimensional rendering of back of breakout board.

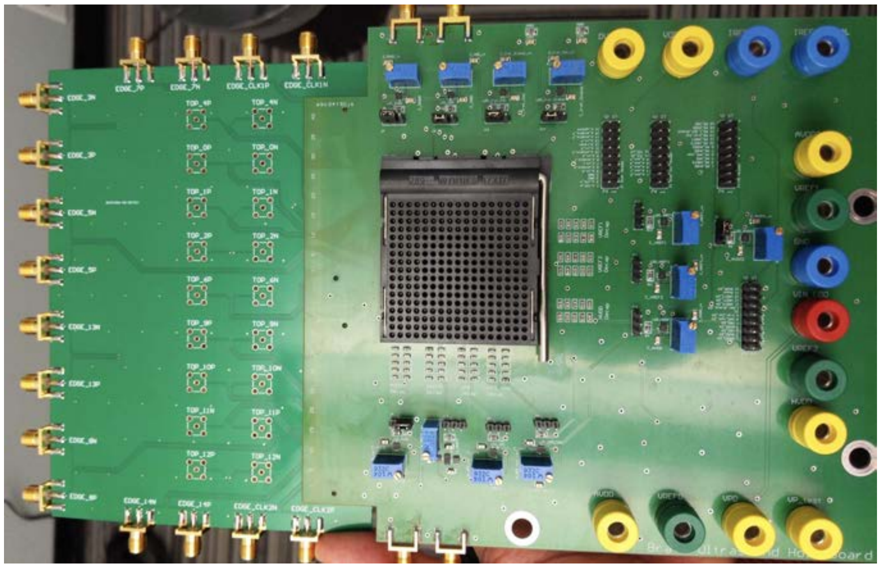

(c) Breakout board (left, without top SMAs soldered) connected to hostboard (right).

Figure 2.4: FMC breakout board.

Figure 2.5 depicts the ultrasound receiver measurement setup. A 3D printed tank made of PLA filament is attached to the chip board using silicone; the pins on the chipboard are covered with silicone as well to isolate them from the water that will fill the tank. The chipboard is attached to the hostboard, which connects to the breakout board via an FMC connector. A laser is parked at the left (stable) flank of the target ring's Lorentzian and is input to the sensing array through an optical fiber. The tank is filled with water and a PMUT excited by either an AWG or an ultrasonic pulser is immersed in the water. Each measurement (a stream of the data packets in Figure 2.3) is captured on the oscilloscope and saved to an external drive for post-processing.

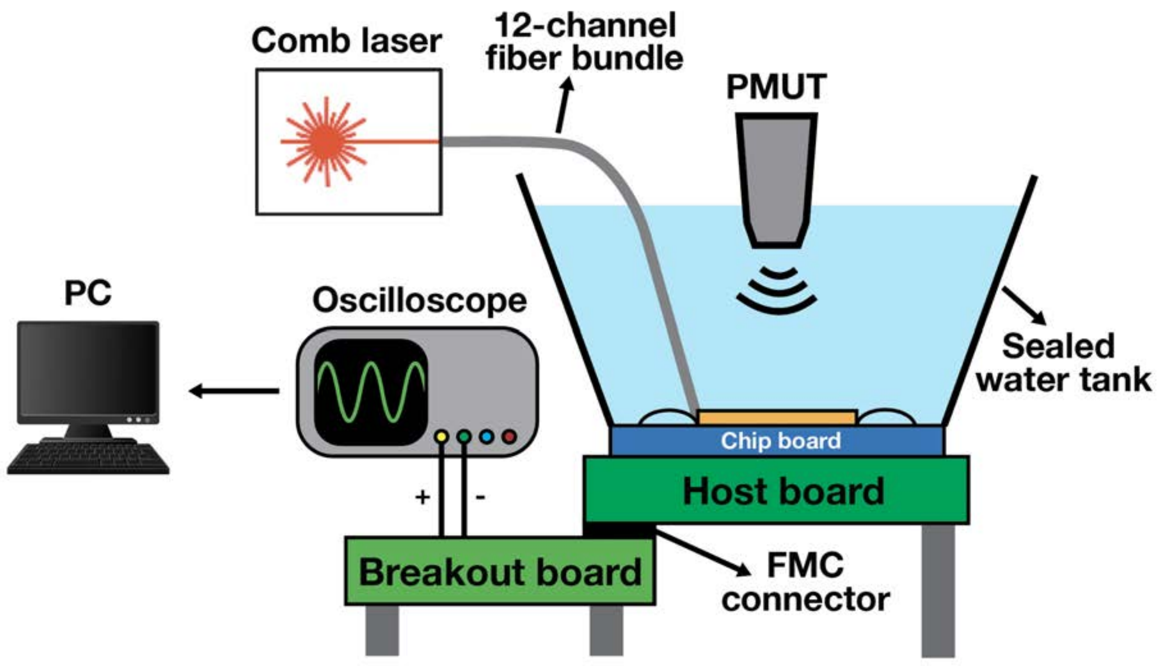

Figure 2.5: Ultrasound measurement setup.

2.2 Ultrasonic measurements

Transducer calibration

The following measurements are included:

1. frequency response of ultrasound transducer,
2. angular response (varying horizontal distance between transducer and hydrophone),
3. and response to varying the vertical distance between the transducer and hydrophone.

The pressure in Pascals is calculated using the following formula:

$$P_{pp}\ [\mathrm{Pa}] = \frac{V_{pp}\ [\mathrm{V}]}{\text{sensitivity}\ [\mathrm{V/Pa}] \cdot G_{\text{pre-amp}}}$$

where V_{pp} is the peak-to-peak voltage of the pre-amplifier output and the hydrophone sensitivity at a particular frequency is given by Onda calibration data. $G_{\text{pre-amp}} = 20$ dB is the voltage gain of the pre-amplifier. Measurements to verify the linear response of each transducer were taken as well by varying the amplitude of the sinusoidal excitation while fixing its frequency.

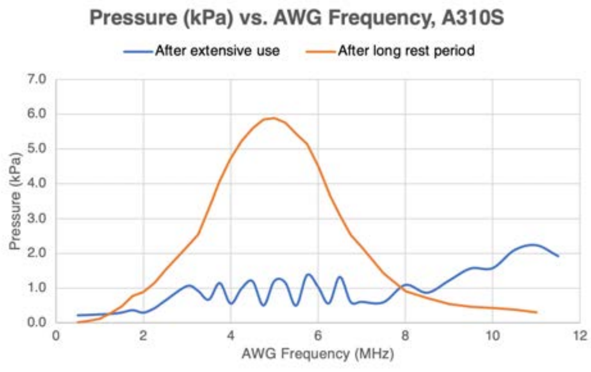

(a) Olympus A310S (5 MHz), $h = 3.2$ cm

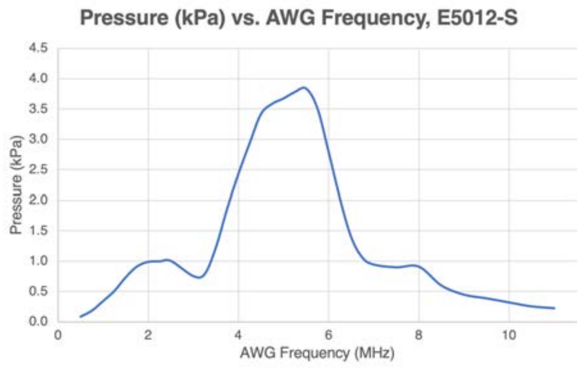

(b) NDT E5012-S (5 MHz), $h = 3.2$ cm

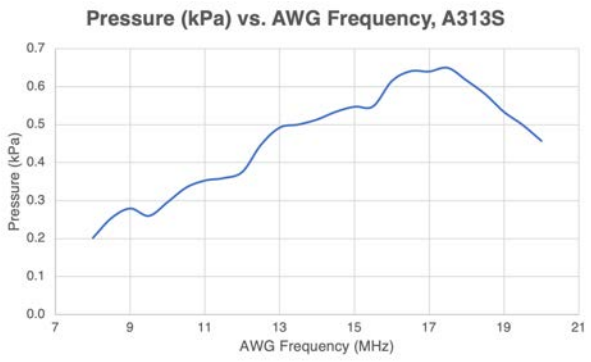

(c) Olympus A313S (15 MHz), $h = 3.2$ cm

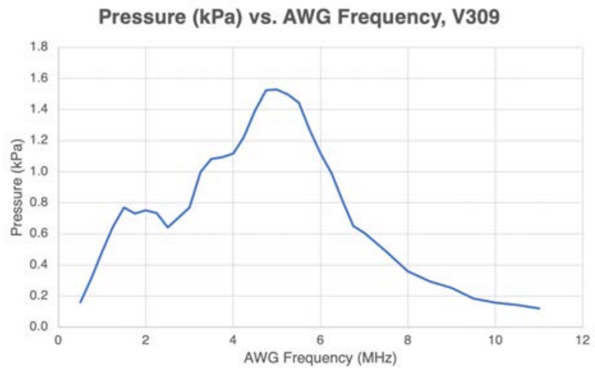

(d) Olympus V309 (5 MHz), $h = 3.2$ cm

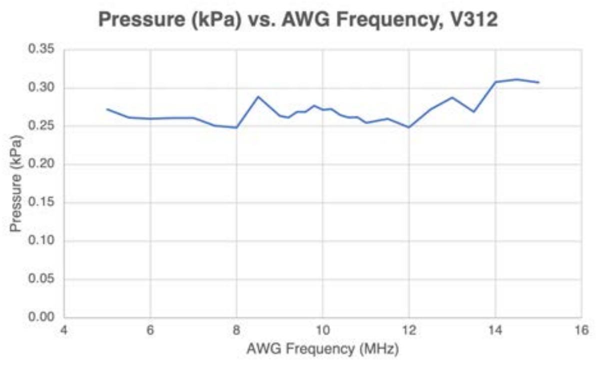

(e) Olympus V312 (10 MHz), $h = 1.6$ cm

Figure 2.6: Transfer functions for various transducers, where h is the vertical distance between each transducer and the hydrophone.

Figure 2.6 includes the frequency response of several immersion PMUTs. Figure 2.6a demonstrates that the transfer function of the immersion transducer degrades with extensive use and requires a rest period after a lengthy period of excitation.

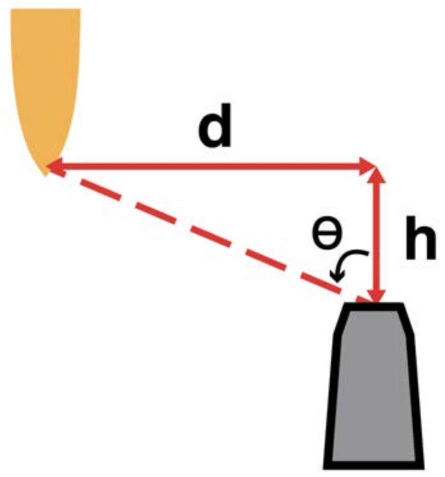

(a) Angular measurement setup.

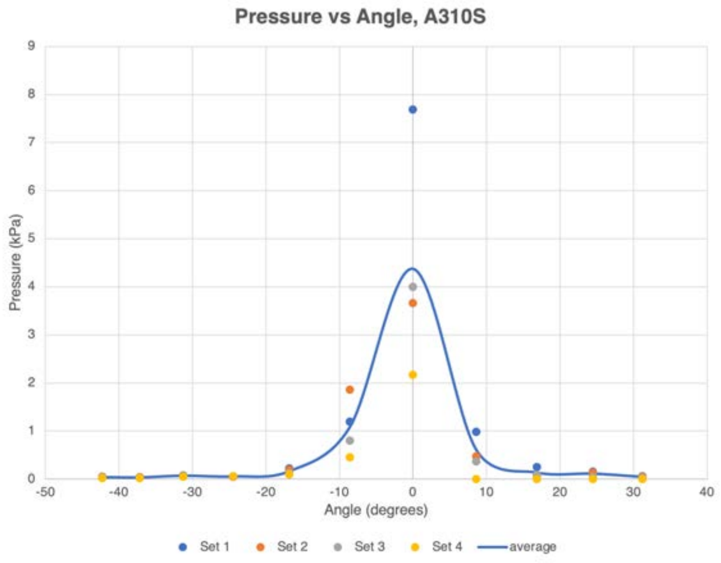

(b) Pressure vs. angle for A310S PMUT, $h = 3.2$ cm.

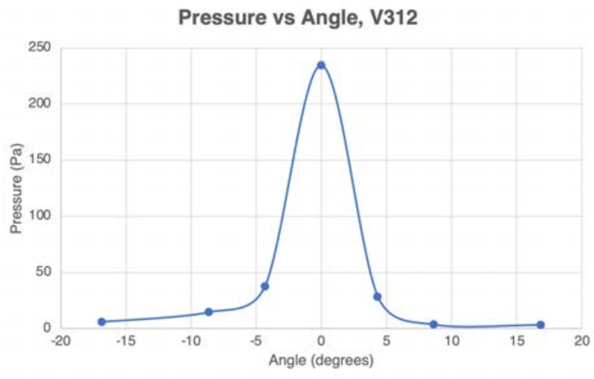

(c) Pressure vs. angle for V312 PMUT, $h = 1.6$ cm.

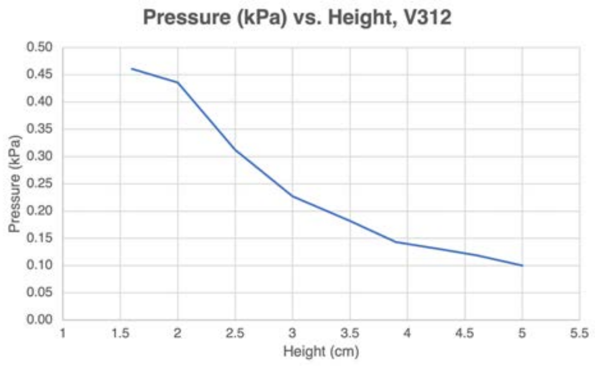

(d) Pressure vs. height for V312 PMUT.

Figure 2.7: Angular measurements.

The adjustable stage in the transducer measurement setup shown in Figure 2.2 has three degrees of freedom — it can be adjusted in the x, y, and z directions. It is difficult to mount the hydrophone such that it can be accurately placed at an angle to the hydrophone while maintaining the same distance between the transducer and the hydrophone. Instead, the setup illustrated by Figure 2.7a is used. The adjustable stage is varied in the y-direction while the x and z directions remain constant. The angle, θ, between the hydrophone and the PMUT is calculated by $\theta = \tan^{-1}\left(\frac{d}{h}\right)$. Measurements were also taken varying h by adjusting the stage only in the z-direction with the hydrophone centered over the transducer in the xy-plane. Figure 2.7 displays the results of these positional measurements. Each measurement was taken by exciting each transducer with a sinusoid at its resonant frequency.

Angular measurements were taken for the A313S transducer as well, but the plot has been omitted since the measured pressure was approximately 851 Pa for all angles.

MRR ultrasound receiver measurements

Bandwidth measurements with external TIA

Bandwidth measurements were taken using an external Thor Labs PD-TIA and measured directly on an oscilloscope. As the frequency of the transducer excitation is swept, the peak-to-peak voltage output of the PD-TIA is measured on the oscilloscope and recorded manually on a PC.

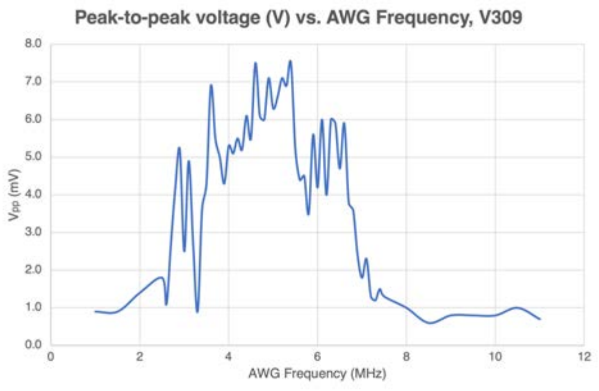

(a) V309 (5 MHz), $h = 1.6$ cm

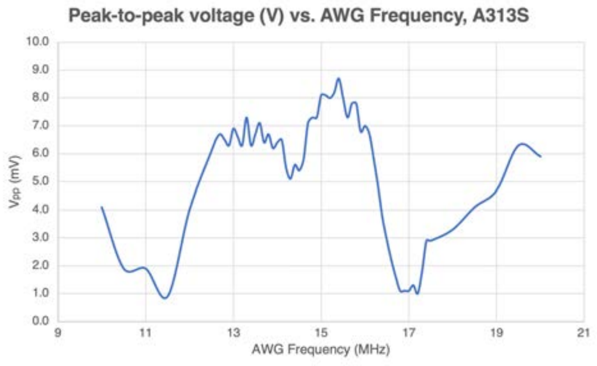

(b) A313S (15 MHz), $h = 1.6$ cm

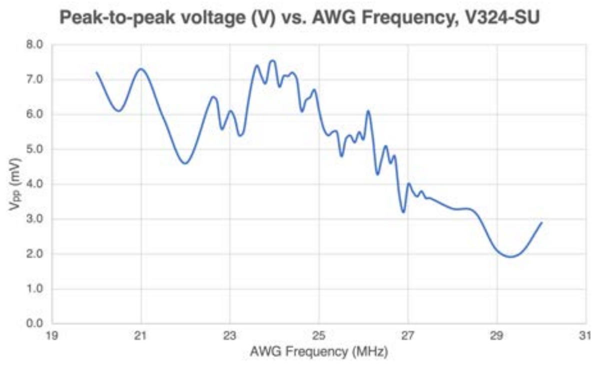

(c) V324-SU (25 MHz), $h = 1.1$ cm

Figure 2.8: Bandwidth measurements using various transducers, where h is the vertical distance between each transducer and the chip and the PMUT is centered over the ring.

Sensing ultrasonic pulse

The oscilloscope waveforms from the setup in Figure 2.5 are parsed using a Python script to recover the received signal from the serial data packets. Figure 2.9 summarizes the script in the form of a block diagram.

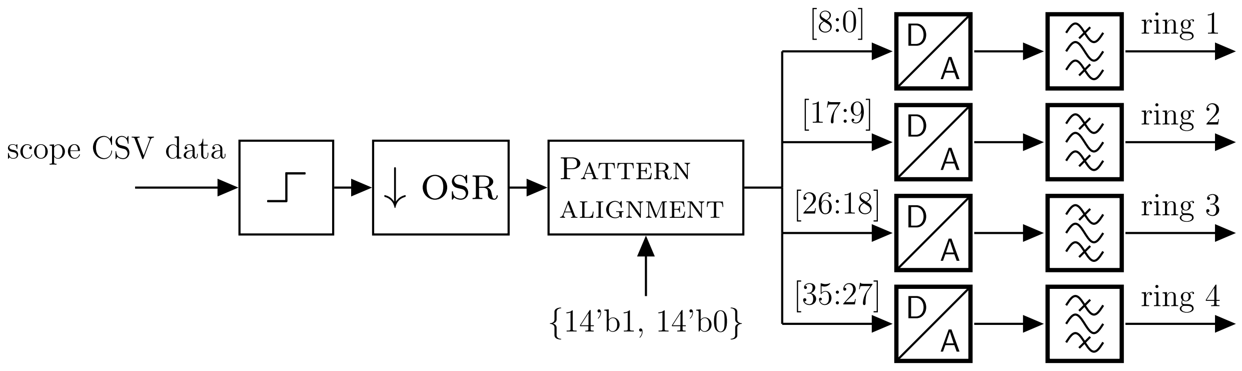

Figure 2.9: Block diagram for oscilloscope data processing code to recover analog data from each ring in a quad.

Explanation of each block:

- ⎍: comparator, outputs 1 if the $\text{scope}_p > \text{scope}_n$ or 0 if $\text{scope}_p < \text{scope}_n$
- ↓ OSR: downsamples the bitstream by the oversampling rate (OSR), which is defined as follows:

$$\text{OSR} = \frac{\text{f}_{\text{sample, scope}}}{2 \cdot \text{f}_{\text{clk, ADC}}}$$

- Pattern alignment: deserializes serial data into 64-bit packets aligned to the 28-bit preamble {14'b1, 14'b0}, isolates the data by keeping only the first 36 bits of each packet, and separating the data into 4 9-bit chunks
- D/A : converts 9-bit binary ADC outputs to decimal (units: SAR least significant bits (LSBs), where 512 LSBs corresponds to the fullscale ADC output)
- ≈ : bandpass finite impulse response (FIR) filter centered at 5 MHz with cutoff frequencies 2.5 MHz and 7.5 MHz

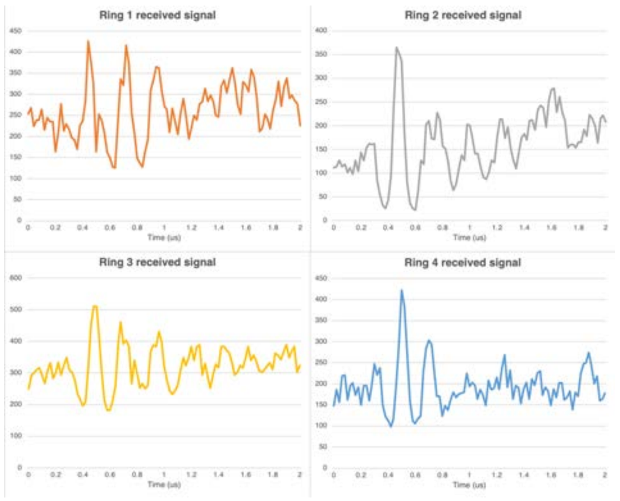

(a) Unfiltered signals.

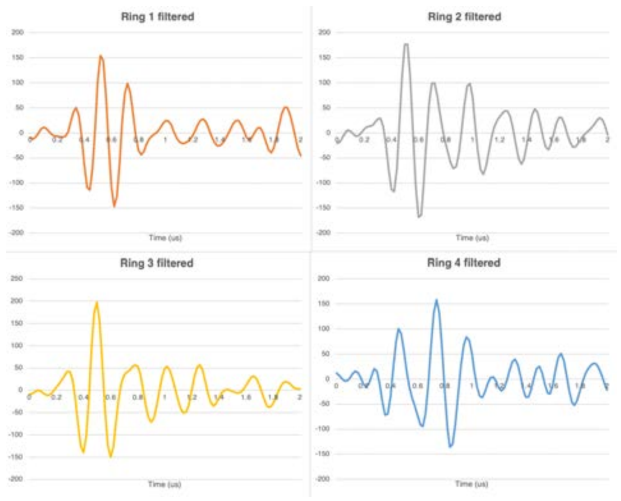

(b) Filtered signals.

Figure 2.10: Received signals recovered from serialized data packets captured on oscilloscope.

Figure 2.10 shows the output of the Python script described in Figure 2.9 for a ring quad with a pulse excitation centered at 5 MHz. Figure 2.10b shows the output of filtering the signals in 2.10a with a 101-tap FIR bandpass filter with cutoff frequencies at 2.5 MHz and 7.5 MHz, which are the assumed lower and upper limits of the frequencies in the pulse.

Bandwidth and sensitivity results

The sensitivity of a ring is calculated using the following formula:

$$\begin{aligned} S &= \frac{\delta V_{out}}{\delta P_{app}} \text{ [V / Pa]} \\ &= \frac{\delta \lambda_{res}}{\delta P_{app}} \frac{\delta P_{opt}}{\delta \lambda_{res}} R_{PD} G_{TIA} \end{aligned}$$

where V_{out} is the measured peak-to-peak output voltage, P_{app} is the pressure applied (calculated using the transducer calibration measurements), λ_{res} is the resonant wavelength of the ring, P_{opt} is the input optical power, R_{PD} is the responsivity of the photodetector, and G_{TIA} is the TIA gain. [7]

A 5MHz sinusoidal excitation yields a fitted peak-to-peak output of 75 LSB codes, so the estimated receiver sensitivity is calculated as follows:

$$\begin{aligned} S &= \frac{600 \text{ mV}}{512 \text{ LSBs}} \cdot 75 \text{ LSBs} \cdot \frac{1}{12.1 \text{ kPa}} \\ &= 7.3 \frac{\text{mV}}{\text{kPa}} \text{ [8]} \end{aligned}$$

where 600 mV is the fullscale output of the 9-bit ADC corresponding to 512 LSB codes and 12.1 kPa is the pressure applied to the chip, back-calculated from the PMUT characterization measurements outlined in the previous section.

The bandwidth of the MRR sensors is $\geq$ 30 MHz (Figure 2.8c). The true bandwidth may be higher than 30 MHz, but the PMUT with the highest resonant frequency used was 25 MHz (V324-SU).

2.3 Electrical measurements

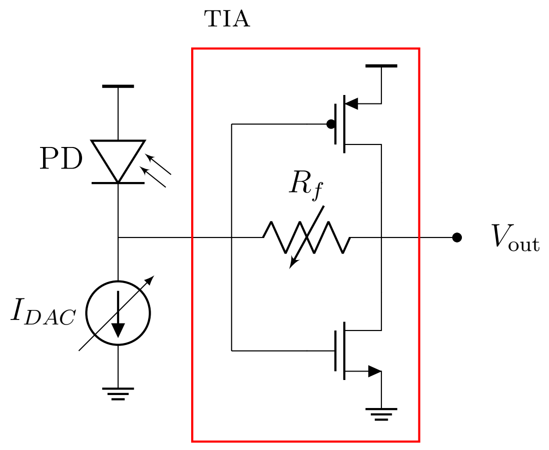

Figure 2.11: Schematic of AFE.

Figure 2.11 depicts part of the analog frontend (AFE). A 5-bit tunable pull-down current digital-to-analog converter (DAC), I_{DAC}, sets the common-mode voltage at the TIA output (V_{out}). The tunable TIA feedback resistor R_f has 4 configuration bits, allowing for 16 gain settings from 50kΩ to 800kΩ. AFE settings such as TIA gain ($\approx R_f$) and I_{DAC} code can be adjusted to optimize the Lorentzian shape for each ring in order to maximize ring sensitivity by maximizing $\frac{\delta P_{opt}}{\delta \lambda_{res}}$. These configuration bits can be updated using a Python script to interface with the scan chain.

```python
all_lorentzians = []  # Define matrix of Lorentzians, where the Lorentzian for gain = i and
    idac = j is located at all_lorentzians[i][j]

for gain in gains:  # Iterate over all possible gain settings
    set_gain(gain)  # Commit gain to scan chain

    lorentzians = []

    for idac in idacs:  # Iterate over all possible idac settings
        set_idac(idac)  # Commit idac code to scan chain

        lorentzian = []  # Define Lorentzian array for the current configuration

        for wavelength in wavelengths:  # Sweep laser over desired range of wavelengths
            laser.set_wavelength(wavelength)
            SAR_output = int(get_scan_chain(ring), 2)  # Scan out ADC output at this
    wavelength, convert to integer
            lorentzian.append(SAR_output)

        lorentzians.append(lorentzian)  # Append Lorentzian for this idac setting

    all_lorentzians.append(lorentzians)  # Append all Lorentzians for this gain setting

slope = [[max(np.diff(j)) / step for j in i] for i in all_lorentzians]  #  Find the maximum
    Lorentzian slope for every configuration

# Finally, find the setting that yields the maximum possible slope

```

Listing 2.1: Pseudocode to find optimal AFE settings, loosely written in Python.

Listing 2.1 contains a simplified version of a Python script that iterates over the gain and I_{DAC} settings to find the optimal configuration. A Lorentzian is found for each AFE setting by sweeping the input laser wavelength around the ring resonance and recording the SAR output through the scan chain.

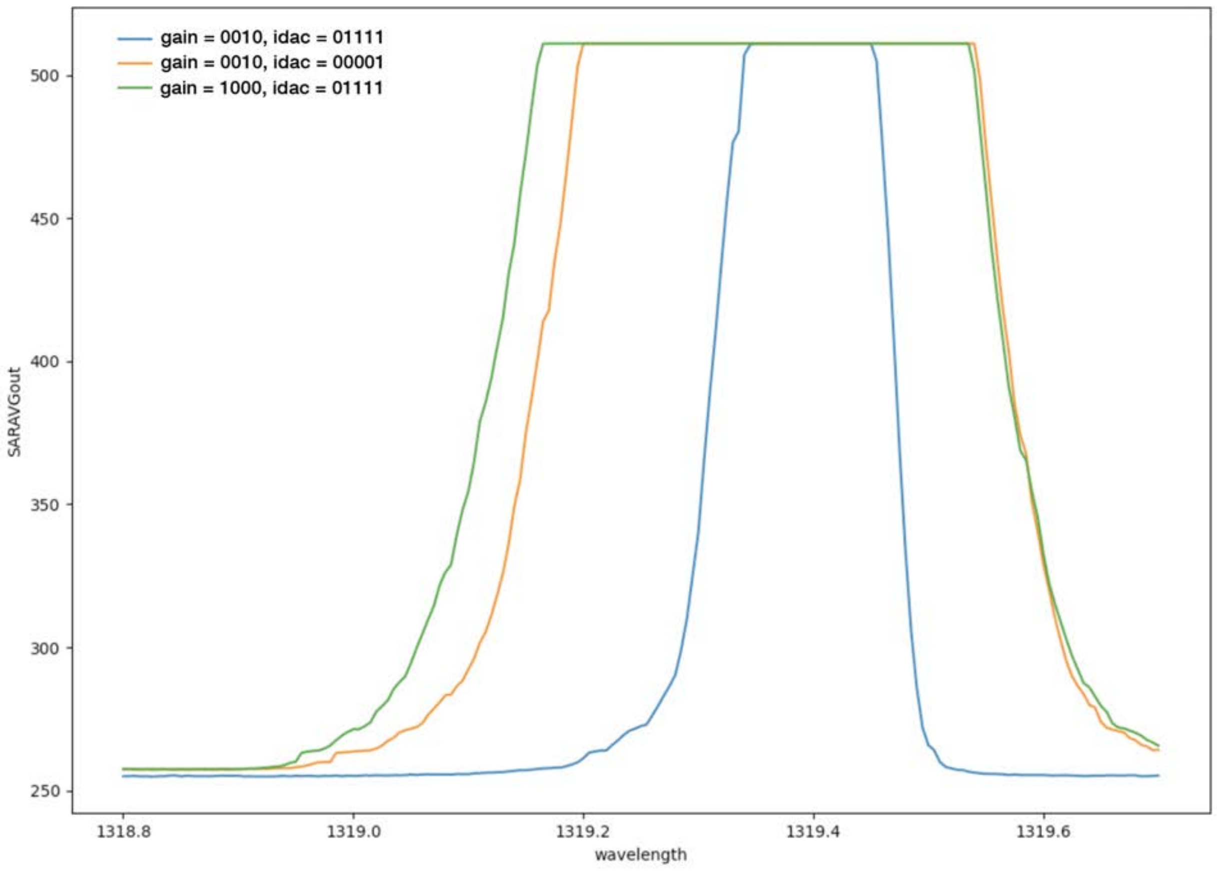

Figure 2.12: Result of gain/I_{DAC} sweeping script.

The output of this sweeping script is plotted in Figure 2.12. The optimal combination of gain and I_{DAC} code is the blue Lorentzian, which has a maximum slope of 5.365 $\frac{\text{SAR LSBs}}{\text{pm}}$. The Lorentzians corresponding to two non-optimal settings have been plotted as well for comparison.

Chapter 3

Photonic Layout

This chapter proposes an automated, fully parameterizable photonic layout design for future generations of the ultrasound sensing chip using a commercial fiber block in order to address the tradeoff between maximizing the number of sensing elements and minimizing the size of the probe tube.

3.1 Berkeley Photonic Generator

Berkeley Photonic Generator (BPG) is a Python-based photonic layout automation tool. BPG enables a user to parameterize a design such that it is easy to generate a new layout by simply changing design parameters.

Each layout can be specified using a Python class with the following methods:

- `get_params_info(cls)`: describes each parameter in the design
- `get_default_param_values(cls)`: returns a dictionary with the default parameter values for the design
- `draw_layout(self)`: instance method that denotes the physical layout of the design

Layouts can be generated hierarchically; a top level `draw_layout(self)` script can instantiate classes corresponding to lower-level layouts defined by the user.

3.2 Fanout for a commercial fiber block

The current layout has receiver arrays with 4 rows of 8 rings per row. To enable higher resolution images in the future, it is vital to implement the following:

1. Significantly reduce the pitch between the MRRs.
2. Increase the total number of rings in the array.

3. Minimize the diameter of the probe tube.

The pitch-reducing optical fiber arrays (PROFAs) proposed by Kopp et. al. [4] enable items 2 and 3. With a minimum of 7 and a maximum of 61 channels, these hexagonal PROFAs can enable a single comb laser input to provide input to anywhere from 6 to 60 ring rows through a tree of 50-50 multi-mode inferometer (MMI) splitters. The unused outputs of the MMI splitter tree can be routed to other couplers to characterize the loss of the MMI tree as well as the MMI splitting capability. Furthermore, since the grating coupler pitch is between 35 and 45 μm, the maximum probe tube diameter is approximately 0.405 mm. This combination of reduced coupler pitch and a large number of channels addresses the tradeoff between minimizing the amount of probe tube cabling and maximizing the number of sensing elements on the probe tip. The face of a PROFA tip with 61 channels is illustrated in Figure 3.1.

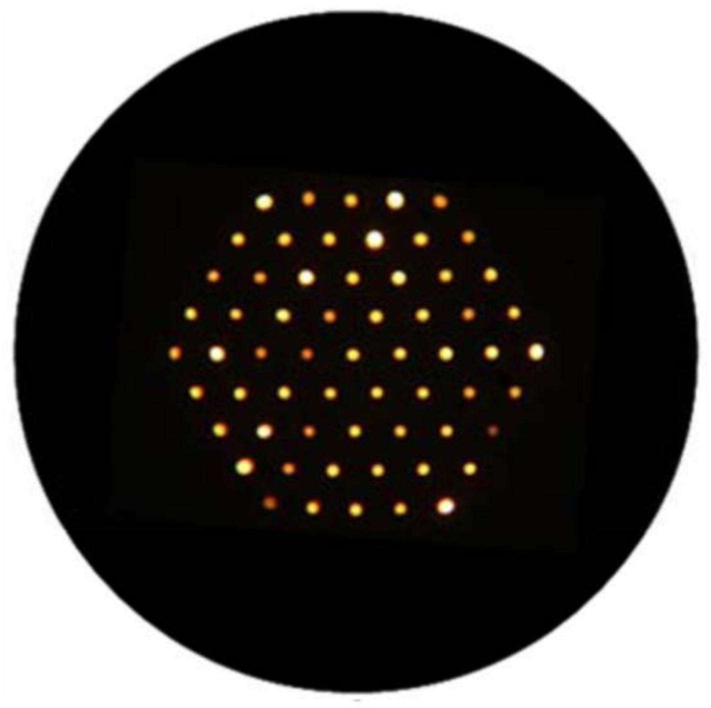

Figure 3.1: Microscope image of the face of the PROFA tip with 61 channels. [4, p. 610]

This chapter details the design and layout of this concept using BPG. This generator lays out a fanout for a PROFA using one fiber as an input and the remaining fibers as outputs, where the fiber pitch and number of fibers are fully parameterizable. The input grating coupler is routed to the input of an MMI splitter tree; each output of the MMI splitter tree is routed to a ring row, the output of which is routed back to the PROFA fanout. The ring array pitch is parameterizable as well.

3.3 Generator design

The hierarchy of the generator is as follows:

```
Top level generator
├──Grating coupler hexagonal array + fanout
└──MMI splitter tree + ring rows
```

Grating coupler hexagonal array + fanout

This generator lays out a hexagonal array of grating couplers with the specified grating coupler pitch; it then fans out the port of each grating coupler to the right using the specified waveguide pitch. The script calculates how many waveguides can fit between two rows of grating couplers, and routes the remaining coupler ports that can't fit between two rows around the fiber block.

Parameter	Description
row_layout_package	Layout package for a ring row
row_class_package	Class package for a ring row
row_params	List of params for a ring row
gc_layout_package	Layout package for the grating coupler
gc_class_package	Class package for the grating coupler
wg_bend_radius	Waveguide bend radius
wg_pitch	Minimum pitch between adjacent waveguides
rout	List of ring radii in a row
gc_pitch	Pitch between grating couplers
min_coupler_row	Number of couplers in the top row of the array

Table 3.1: Fiber array fanout parameters.

`draw_layout(self)` code:

```
gc_pitch = self.params['gc_pitch']
min_coupler_row = self.params['min_coupler_row']
wg_pitch = self.params['wg_pitch']
wg_bend_radius = self.params['wg_bend_radius']

num_rows = 2 * min_coupler_row - 1

gc_layout_package = self.params['gc_layout_package']
gc_cls_name = self.params['gc_class_package']

gc_lay_module = importlib.import_module(gc_layout_package)
gc_cls = getattr(gc_lay_module, gc_cls_name)

gc_master = self.new_template(params=dict(), temp_cls=gc_cls)

num_couplers = min_coupler_row
start_offset_x = 0
```

```
offset_y = 0

# Calculate maximum number of waveguides that will fit between coupler rows
max_wgs = math.floor(gc_pitch / np.sqrt(2) / wg_pitch) - 1
around_offset_y = min(num_couplers - 1, max_wgs - 1) * wg_pitch \
    + wg_pitch - 2 * wg_bend_radius
around_offset_x = gc_pitch

end_x = (2 * min_coupler_row - 1) * gc_pitch

idx = 0
min_actual_y = 0

top_gc_rows = []
bottom_gc_rows = []

# Iterate over array rows to generate grating coupler array
for i in range(num_rows):
    dir = 1
    num_around = num_couplers - max_wgs - 1

    # Iterate over all grating couplers in a row
    for j in range(num_couplers):
        if i < min_coupler_row - 1:
            dir = -1
        elif i > min_coupler_row - 1:
            dir = 1
        offset_x = start_offset_x + j * gc_pitch
        gc_inst = self.add_instance(master=gc_master,
                                    loc=(offset_x, offset_y),
                                    orient='R180')
        gc_port = gc_inst['INPUT']

        # Begin route at output of grating coupler
        router = WgRouter(gen_cls=self, init_port=gc_port,
                          layer=('rx1phot', 'drawing'), name='route{}{}'.format(i, j),
                          wg_params={'bend_type': 'trajECE', 'radius': wg_bend_radius,
                                     'AngleTurnEuler': .5})
        if dir == 1:
            dir1 = 'left'
            dir2 = 'right'
        else:
            dir2 = 'left'
            dir1 = 'right'

        # Last coupler in a row
        if j == num_couplers - 1:
            loc = router.port.center
            router.cardinal_router(points=[(end_x, loc[1])],
                                   bend_params=dict(radius=wg_bend_radius,
                                                    bend_type='trajCirc'))
            if i == min_coupler_row - 1:
                router_start = router

        # Can't fit all waveguides between rows
        elif (j < num_couplers - max_wgs - 1 and i != min_coupler_row - 1) \
            or (i == min_coupler_row - 1 and (num_couplers - j) // 2 > max_wgs):
            if dir == 1:
                around_offset_x = around_offset_x - wg_pitch
                around_offset_y = around_offset_y

            dist = 1 + j * wg_pitch
            (router
```

```python
             .add_straight_wg(length=0.5)
             .add_90_bend(direction=dir1,
                          bend_params=dict(radius=wg_bend_radius, bend_type='circular'))
             .add_straight_wg(length=dist))
            loc = router.port.center
            if i == min_coupler_row - 1:
                num_around = num_couplers - 2 * max_wgs
                if dir == -1:
                    actual_x = around_offset_x + (num_around - 1 - 2 * j // 2) * wg_pitch
                    actual_y = around_offset_y - 2 * wg_bend_radius + i * gc_pitch / \
                        np.sqrt(2) + wg_pitch * (idx - 3 * j // 2 + num_around - 1)
                else:
                    actual_x = around_offset_x + wg_pitch
                    actual_y = around_offset_y - 2 * wg_bend_radius + (num_rows - 1 - i) \
                        * gc_pitch / np.sqrt(2) + wg_pitch * (- j // 2 + idx + 1)
            elif dir == -1:
                actual_x = around_offset_x + (num_around - 1 - 2 * j) * wg_pitch
                actual_y = around_offset_y - 2 * wg_bend_radius + i * gc_pitch / np.sqrt(
                    2) + wg_pitch * (idx - 3 * j + num_around)
            else:
                actual_x = around_offset_x
                actual_y = around_offset_y - 2 * wg_bend_radius + (num_rows - 1 - i) * \
                    gc_pitch / np.sqrt(2) + wg_pitch * (-j + idx)
            if loc[0] > -around_offset_x:
                if dir == 1:
                    idx -= 1
                router.add_90_bend(direction=dir1,
                                   bend_params=dict(radius=wg_bend_radius,
                                                    bend_type='circular'))
                loc = router.port.center
                (router
                    .cardinal_router(points=[(-actual_x + wg_bend_radius, loc[1])],
                                     bend_params=dict(radius=wg_bend_radius,
                                                      bend_type='trajCirc'))
                    .add_90_bend(direction=dir2, bend_params=dict(radius=wg_bend_radius,
                                                                  bend_type='circular'))
                    .add_straight_wg(length=actual_y)
                    .add_90_bend(direction=dir2, bend_params=dict(radius=wg_bend_radius,
                                                                  bend_type='circular')))
                loc = router.port.center
                router.cardinal_router(points=[(end_x, loc[1])],
                                       bend_params=dict(radius=wg_bend_radius,
                                                        bend_type='trajCirc'))
                if dir == -1:
                    idx += 1
            else:
                (router
                    .add_straight_wg(length=around_offset_y + min(i, num_rows - 1 - i)
                                     * gc_pitch / np.sqrt(2))
                    .add_90_bend(direction=dir2,
                                 bend_params=dict(radius=wg_bend_radius,
                                                  bend_type='circular')))
                loc = router.port.center
                router.cardinal_router(points=[(end_x, loc[1])],
                                       bend_params=dict(radius=wg_bend_radius,
                                                        bend_type='trajCirc'))

            if actual_y > min_actual_y and dir == -1:
                min_actual_y = actual_y
            if dir == -1:
                around_offset_x = around_offset_x + wg_pitch
                around_offset_y = around_offset_y

```

```
        # Can fit waveguide between rows
        else:
            if i == min_coupler_row - 1:
                dist = 1 + (num_couplers - j - 2) // 2 * wg_pitch + wg_pitch - \
                    2 * wg_bend_radius
            else:
                dist = 1 + (num_couplers - j - 2) * wg_pitch + wg_pitch - 2 * wg_bend_radius
            (router
             .add_straight_wg(length=0.5)
             .add_90_bend(direction=dir1,
                          bend_params=dict(radius=wg_bend_radius, bend_type='circular'))
             .add_straight_wg(length=dist)
             .add_90_bend(direction=dir2,
                          bend_params=dict(radius=wg_bend_radius, bend_type='circular')))
            loc = router.port.center
            router.cardinal_router(points=[(end_x, loc[1])],
                                   bend_params=dict(radius=wg_bend_radius,
                                                    bend_type='trajCirc'))
        if dir == 1:
            top_gc_rows.append(router)
        else:
            bottom_gc_rows.append(router)
        dir = -dir

    if i < min_coupler_row - 1:
        start_offset_x = start_offset_x - gc_pitch / 2
        num_couplers = num_couplers + 1
    else:
        start_offset_x = start_offset_x + gc_pitch / 2
        num_couplers = num_couplers - 1
    offset_y = offset_y + gc_pitch * 1 / np.sqrt(2)

top_gc_rows = sorted(top_gc_rows, key=lambda x: x.port.center[1])
bottom_gc_rows = sorted(bottom_gc_rows, key=lambda x: x.port.center[1])

# Extract output ports
for idx, row in enumerate(top_gc_rows):
    row.extract_port('TOP_' + str(idx))

for idx, row in enumerate(bottom_gc_rows[::-1]):
    row.extract_port('BOTTOM_' + str(idx))

# Extract input port
router_start.extract_port('CENTER')
```

Listing 3.1: Generator for grating coupler fanout.

MMI splitter tree + ring rows

This generator lays out a binary MMI splitter tree based on the number of possible outputs in the fiber array fanout. It calculates the tree depth as follows:

$$\text{depth} = \lceil \log_2 n \rceil$$

where n is the number of outputs. It then lays out n MRR rows, which means that there are $2^{\text{depth}} - n$ unused splitter tree outputs.

Parameter	Description
switch_tree_layout_package	Layout package for the binary switch tree
switch_tree_class_package	Class package for the binary switch tree
switch_elem_pitch	Element pitch for the binary switch tree
row_layout_package	Layout package for a ring row
row_class_package	Class package for a ring row
row_params	List of params for a ring row
wg_pitch	Minimum pitch between adjacent waveguides
wg_bend_radius	Waveguide bend radius
contact_name_start_ind	The start index for contact label names
num_rings_per_row	The number of rings per row in this array
coupling_gap_base_1	Initial coupling gap of left array
coupling_gap_pitch_1	Pitch with which coupling gap increments - left array
rout	List of ring radii in a row
min_coupler_row	Number of couplers in the top row of the array

Table 3.2: MMI splitter tree + ring rows parameters.

`draw_layout(self)` code:

```python
switch_tree_layout_package = self.params['switch_tree_layout_package']
switch_tree_cls_name = self.params['switch_tree_class_package']

switch_tree_lay_module = importlib.import_module(switch_tree_layout_package)
switch_tree_cls = getattr(switch_tree_lay_module, switch_tree_cls_name)

row_layout_package = self.params['row_layout_package']
row_cls_name = self.params['row_class_package']

row_lay_module = importlib.import_module(row_layout_package)
row_cls = getattr(row_lay_module, row_cls_name)

min_coupler_row = self.params['min_coupler_row']

# Add routes, ring rows, and grating couplers
num_rows = 3 * sum([2 * i for i in range(1, min_coupler_row)])

tree_depth = math.ceil(math.log2(num_rows))
row_offset = (2 ** tree_depth - num_rows) // 2
```

```
num_rings_tot = num_rows * self.params['num_rings_per_row'] - 1

switch_tree_params = dict(element_pitch=self.params['switch_elem_pitch'],
                          input_port_name='IN_TOP', tree_depth=tree_depth)

switch_tree_master = self.new_template(params=switch_tree_params, temp_cls=switch_tree_cls)
switch_tree_inst_left = self.add_instance(master=switch_tree_master, loc=(0, 0))

self.extract_photonic_ports(inst=switch_tree_inst_left, port_names=['INPUT'])

contact_name_ind = 0

for ind in range(num_rows):

    curr_dict = deepcopy(self.params["row_params"])
    name_str = 'Mod1_'
    coupling_gap_var = dict(
        ring_params_list=[dict(rout=self.params['rout'][x],
                               coupling_slot=self.params['coupling_gap_base_1'] + x *
                               self.params['coupling_gap_pitch_1']) for x in
                          range(self.params['num_rings_per_row'])])

    contact_name_dict = dict(
        ring_labels=[dict(N=name_str + 'RingCat' + '<' + str(num_rings_tot - x) + '>',
                          P=name_str + 'RingAn' + '<' + str(num_rings_tot - x) + '>') for
                     x in range(contact_name_ind, contact_name_ind
                                + self.params['num_rings_per_row'], 1)],
        heater_labels=[dict(N=name_str + 'HeaterP' + '<' + str(num_rings_tot - x) + '>',
                            P=name_str + 'HeaterN' + '<' + str(num_rings_tot - x) + '>') for
                       x in range(contact_name_ind, contact_name_ind
                                  + self.params['num_rings_per_row'], 1)])

    if ind % 2 == 1:
        contact_name_dict['ring_labels'].reverse()
        contact_name_dict['heater_labels'].reverse()

    curr_dict.update(contact_name_dict)
    contact_name_ind += self.params['num_rings_per_row']

    curr_dict.update(coupling_gap_var)

    row_master = self.new_template(params=curr_dict, temp_cls=row_cls)

    switch_port = switch_tree_inst_left['OUTPUT_' + str(ind + row_offset)]

    router = WgRouter(gen_cls=self,
                      init_port=switch_port,
                      layer=('rx1phot', 'drawing'),
                      name='route' + str(ind + 1))

    row_inst = self.add_instance_port_to_port(inst_master=row_master,
                                              instance_port_name='PORT1',
                                              self_port=router.port,
                                              reflect=True)

    self.extract_photonic_ports(inst=row_inst, port_names=['PORT0'],
                                port_renaming={'PORT0': 'OUTPUT_{}'.format(ind + 1)})
```

Listing 3.2: Generator for splitter tree + ring rows.

Top-level generator

The top-level generator instantiates the fiber array as well as the MMI splitter tree and ring rows. It then iteratively routes all ring row outputs back to the ports of the grating coupler fanout.

Parameter	Description
fiber_arr_layout_package	Layout package (path) to the fiber array
fiber_arr_class_package	Class package (class name) to the fiber array
fiber_arr_params	dict of params for the fiber array
splitter_rows_layout_package	Layout package (path) to the splitter + ring rows
splitter_rows_class_package	Class package (class name) to the splitter + ring rows
wg_bend_radius	Radius of the waveguide bends
wg_width	Waveguide width
wg_pitch	Minimum waveguide pitch
min_coupler_row	Number of couplers in the top row of the array

Table 3.3: Top level parameters.

`draw_layout(self)` code:

```python
# Add fiber array first as (0, 0)
fiber_arr_layout_package = self.params['fiber_arr_layout_package']
fiber_arr_cls_name = self.params['fiber_arr_class_package']

gen_params = dict(min_coupler_row=self.params['min_coupler_row'], wg_pitch=self.params['
    wg_pitch'])

fiber_arr_lay_module = importlib.import_module(fiber_arr_layout_package)
fiber_arr_cls = getattr(fiber_arr_lay_module, fiber_arr_cls_name)

fiber_arr_master = self.new_template(params=gen_params, temp_cls=fiber_arr_cls)
fiber_arr_inst = self.add_instance(master=fiber_arr_master, loc=(0, 0))

# Calculating total number of ring rows and MMI splitter tree depth
num_rows = 3 * sum([2 * i for i in range(1, fiber_arr_master.params['min_coupler_row'])])
tree_depth = math.ceil(math.log2(num_rows))

wg_pitch = self.params['wg_pitch']

# Route center-most grating coupler to input of MMI splitter tree
router = WgRouter(gen_cls=self,
                  init_port=fiber_arr_inst['CENTER'],
                  layer=('rx1phot', 'drawing'),
                  name='route0',
                  wg_params={'bend_type': 'trajECE', 'radius': 10, 'AngleTurnEuler': .5})

splitter_rows_layout_package = self.params['splitter_rows_layout_package']
splitter_rows_cls_name = self.params['splitter_rows_class_package']

splitter_rows_lay_module = importlib.import_module(splitter_rows_layout_package)
splitter_rows_cls = getattr(splitter_rows_lay_module, splitter_rows_cls_name)

```

```
splitter_rows_master = self.new_template(params=gen_params, temp_cls=splitter_rows_cls)

row_pitch = splitter_rows_master.params['switch_elem_pitch']

router.add_straight_wg(length=50 + num_rows // 2 * wg_pitch)
router.add_s_bend(length=30, shift_left=row_pitch // 2)

splitter_rows_inst = self.add_instance_port_to_port(inst_master=splitter_rows_master,
                                                    instance_port_name='INPUT',
                                                    self_port=router.port)

row_offset = (2 ** tree_depth - num_rows) // 2  # Calculate number of unused splitter
    outputs

# Route all ring row outputs to fiber array fanout
for route_num in range(1, num_rows + 1):
    if route_num < (num_rows) // 2 + 1:
        dir = 'left'
        out_len = route_num + 1
        row = fiber_arr_inst['TOP_{}'.format(route_num)]
        end_y = row.center[1]
    else:
        dir = 'right'
        out_len = num_rows - route_num + 2
        row = fiber_arr_inst['BOTTOM_{}'.format(num_rows - route_num)]
        end_y = row.center[1]

    router = WgRouter(gen_cls=self,
                      init_port=splitter_rows_inst['OUTPUT_{}'.format(route_num)],
                      layer=('rx1phot', 'drawing'),
                      name='route0',
                      wg_params={'bend_type': 'trajECE', 'radius': 10, 'AngleTurnEuler':
    .5})

    (router
     .add_straight_wg(length=wg_pitch)
     .add_straight_wg(length=wg_pitch * out_len)
     .add_90_bend(direction=dir,
                  bend_params=dict(radius=self.params['wg_bend_radius'], bend_type='circular
    '))
     .add_straight_wg(length=100 + (out_len + row_offset) * row_pitch + out_len * wg_pitch)
     .add_90_bend(direction=dir,
                  bend_params=dict(radius=self.params['wg_bend_radius'], bend_type='circular
    '))
     .add_straight_wg(length=row_pitch * splitter_rows_master.params['num_rings_per_row']
                             + 2 * out_len * wg_pitch + 90 * tree_depth)
     .add_90_bend(direction=dir,
                  bend_params=dict(radius=self.params['wg_bend_radius'], bend_type='circular
    ')))

    diff = abs(router.port.center[1] - end_y) - 2 * self.params['wg_bend_radius']

    (router
     .add_straight_wg(length=diff)
     .cardinal_router(points=[row.center],
                      bend_params=dict(radius=self.params['wg_bend_radius'], bend_type='
    trajCirc')))
```

Listing 3.3: Generator for top level layout.

3.4 Generated layouts

Figure 3.2 displays fanouts for PROFA tips of different sizes with the grating couplers omitted. Figure 3.2a has 19 channels with `wg_pitch` = 5 μm, Figure 3.2b has 37 channels with a waveguide pitch of 5 μm, and Figure 3.2c has 61 channels with `wg_pitch` = 6 μm. The grating coupler pitch for each fanout is 40 μm. Note that all the coupler outputs that do not fit between coupler rows are routed around the fiber block. Therefore, the maximum `wg_pitch` is reached when the total number of couplers is equal to 2· `max_wgs`, where `max_wgs` (see line 21 in Listing 3.1) is the maximum number of waveguides that will fit between coupler rows with the given `gc_pitch` and `wg_pitch`. Using too small a value for `wg_pitch` may result in unwanted coupling. The reduced pitch between the couplers limits the maximum waveguide bend radius (`wg_bend_radius`) as well, which could potentially result in lossy waveguides.

Figure 3.3 displays the generated top-level layouts for each possible number of PROFA channels. In each image, the coupler array and fanout (with couplers omitted) is at the bottom. The coupler output at the center of the fanout routes to the input of the MMI splitter tree in the middle of the image. The MMI splitter outputs route to the ring rows at the top of the image; the ring row outputs are then routed back to the coupler fanout. In each generated layout, `num_rings_per_row` = 16, `wg_pitch` = 5 μm, and the pitch between rings (`switch_elem_pitch`) is 50μm.

Feature	**Current fiber block**	**PROFA**
Number of input couplers	1	1
Number of output couplers/ring rows	4	6-60
Grating coupler pitch	250μm	35-45μm
Ring pitch	220μm	50μm
Total number of rings	32	96-960
Approximate sensing array dimensions	0.75mm x 1.54mm	0.75mm x 0.25mm-2.95mm

Table 3.4: Current fiber block vs. PROFA implementation (assuming the PROFA implementation uses 16 rings per row).

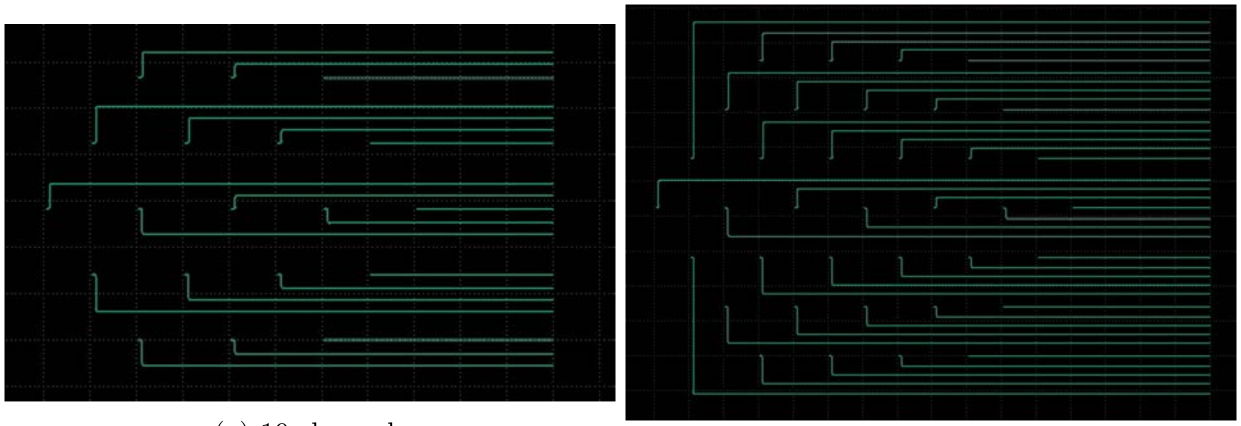

(a) 19 channels

(b) 37 channels

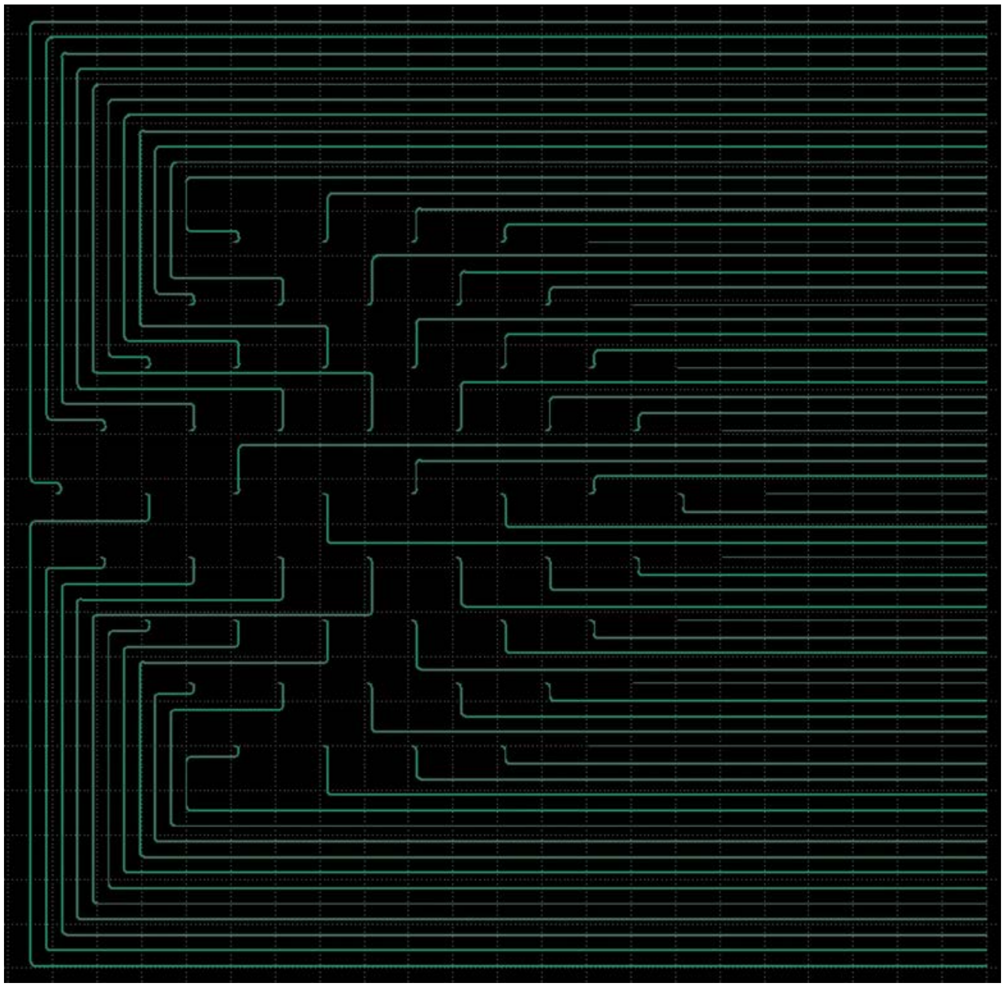

(c) 61 channels

Figure 3.2: BPG generated fanouts for PROFA fiber blocks.

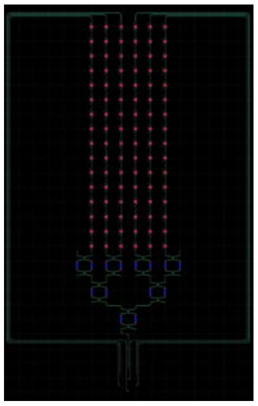

(a) 7 channels

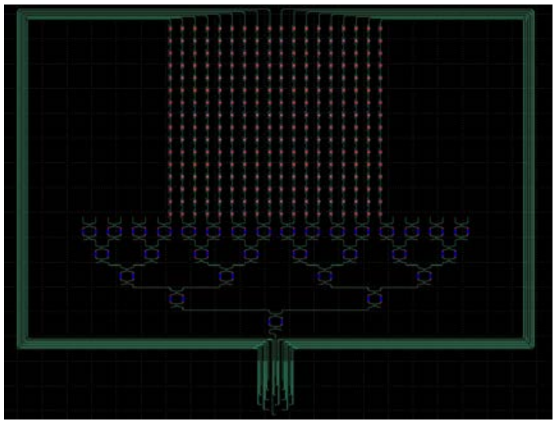

(b) 19 channels

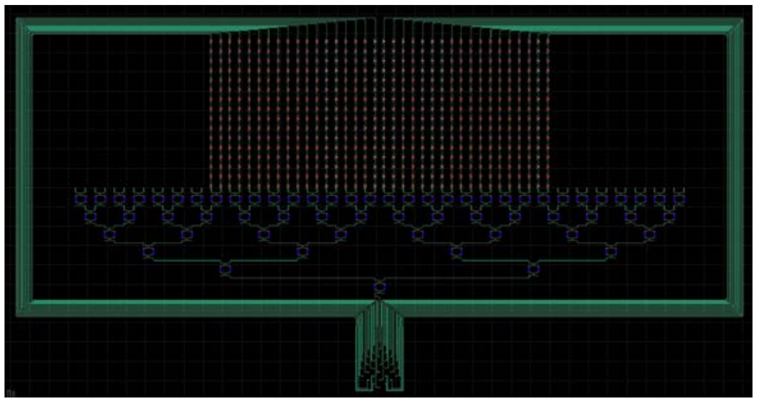

(c) 37 channels

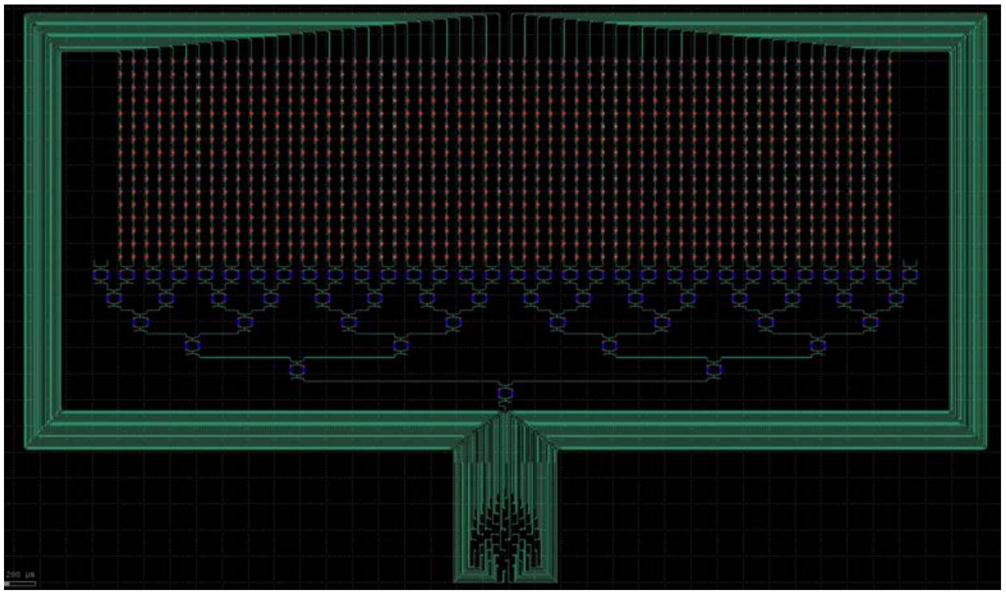

(d) 61 channels

Figure 3.3: BPG generated top level layouts to sense ultrasound with PROFA fiber blocks.

Chapter 4

Analog Frontend Redesign

This chapter explores a potential alternate transimpedance amplifier (TIA) implementation for the chip analog frontend (AFE). It is important to minimize TIA noise to avoid thermal noise from the metal-oxide-semiconductor field-effect transistors (MOSFETs) dominating the system over the shot noise from the photodetector; it is also desirable to maximize the TIA's open-loop voltage gain A_V. The gain $\frac{V_{out}}{I_{in}}$ of a TIA is defined as follows:

$$G_{TIA} = -\frac{A_V}{1 + A_V} R_f$$

Therefore, as $A_V \to \infty$, $G_{TIA} \to -R_f$, where R_f is the feedback resistance.

4.1 Existing Topology

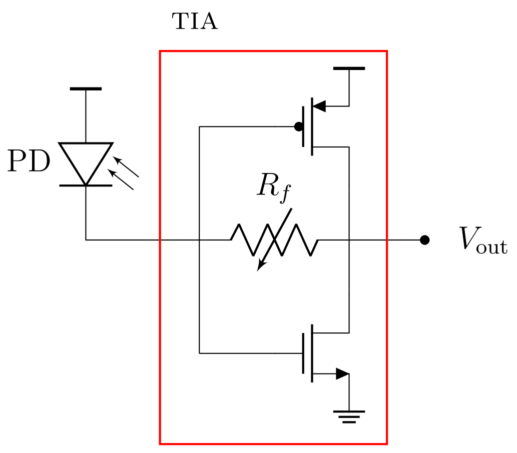

Figure 4.1: Schematic of current AFE implementation.

The existing AFE consists of a MRR photodetector (PD) in series with an inverter-based TIA with a variable feedback resistance R_f. The schematic for the existing AFE is illustrated in Figure 4.1.

This TIA is a **current-reuse** TIA; as the input is connected to the gates of both the NMOS and the PMOS, the effective transconductance G_m is the sum of the NMOS and PMOS g_m's. For the following analysis, the DC operation points g_m and r_o are approximated to be the same for the NMOS and the PMOS.

Gain analysis

To find the gain ($V_{\text{out}}/I_{\text{in}}$) of the TIA, the voltage gain $A_V = G_m R_{\text{out}}$ is found first in order to evaluate the TIA gain as follows:

$$\frac{V_{\text{out}}}{I_{\text{in}}} = -\frac{A_V}{1+A_V}R_f = -\frac{G_m R_{\text{out}}}{1+G_m R_{\text{out}}}R_f$$

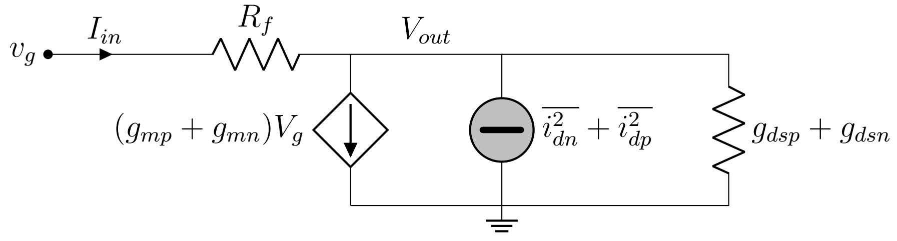

Figure 4.2: Small signal model of current TIA implementation with equivalent noise generator, where $\overline{i_{dn}^2} = 4kT\gamma g_{mn}\Delta f$ and $\overline{i_{dp}^2} = 4kT\gamma g_{mp}\Delta f$.

By inspection of figure 4.2, the effective transconductance G_m of the circuit is $g_{mp}+g_{mn}$ and the output resistance $R_{\text{out}} = r_{op}||r_{on} = (g_{dsp}+g_{dsn})^{-1}$. Therefore,

$$\begin{aligned}\frac{V_{\text{out}}}{I_{\text{in}}} &= -\frac{(g_{mp}+g_{mn})(r_{op}||r_{on})}{1+(g_{mp}+g_{mn})(r_{op}||r_{on})}R_f \\ &\approx -\frac{2g_m\cdot\frac{1}{2}r_o}{1+2g_m\cdot\frac{1}{2}r_o}R_f \\ &\approx -\frac{g_m r_o}{1+g_m r_o}R_f\end{aligned}$$

Noise spectral density analysis

Ignoring the thermal noise from the feedback resistor, the total noise due to the thermal noise from the MOSFETs at the output is as follows:

$$\begin{aligned}
\overline{i^2_{\text{noise, out}}} &= \overline{i^2_{dn}} + \overline{i^2_{dp}} \\
&= 4kT\gamma(g_{mn} + g_{mp})\Delta f \\
\rightarrow \overline{v^2_{\text{noise, out}}} &= \overline{i^2_{\text{noise, out}}} \cdot R^2_{\text{out}} \\
&= 4kT\gamma \frac{g_{mn} + g_{mp}}{(g_{dsp} + g_{dsn})^2}\Delta f \\
&\approx 2kT\gamma g_m r_o^2 \Delta f
\end{aligned}$$

4.2 Proposed Topology

The proposed TIA topology for the AFE is utilized in the piezoelectric ultrasound imaging scheme presented by D'Urbino et al [3]. It is illustrated in Figure 4.3 with feedback resistor and photodetector omitted. A feedback resistor R_f is connected between V^- and V_{out}. The photodetector output is routed to V^- and V^+ is connected to a reference voltage (V_{ref}). This TIA is also a current-reuse TIA, so the effective transconductance G_m will be approximately the sum of the NMOS and PMOS g_m's. Unlike the existing TIA topology, this has a differential input.

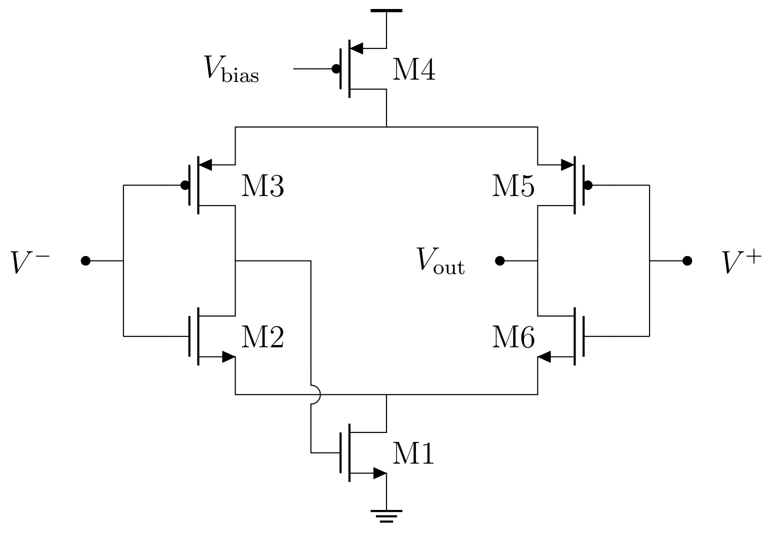

Figure 4.3: Schematic of proposed AFE implementation with feedback resistor omitted.

For the following analysis, g_m and r_o are assumed to be the same for M2, M3, M5, and M6. M1 and M4 are assumed to have the same g_m (but different from the g_m of the complementary transistors, as M1 and M4 are assumed to be in triode). Since M1 and M4 are assumed to be in triode, they can be replaced with resistances $R_{on,p}$ and $R_{on,n}$. The effect of the feedback from the drains of M2 and M3 to the gate of M1 is assumed to be negligible.

Gain analysis

Transconductance

To find the transconductance G_m, the output is shorted and a differential input ($V^+ = \frac{1}{2}v_{id}, V^- = -\frac{1}{2}v_{id}$) is applied to the circuit. G_m is evaluated as the output current I_{out} divided by v_{id}. The node between the sources of M3 and M5 is incremental ground because M3 and M5 have equal and opposite currents due to the differential input. The node between the sources of M3 and M6 is incremental ground for the same reason. This means that the circuit can be split into two differential half-circuits. Figure 4.4 displays the righthand half circuit.

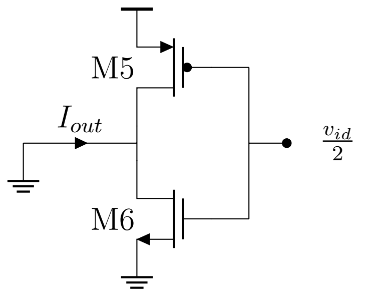

Figure 4.4: Schematic for G_m calculation.

$$\begin{aligned} I_{out} &= g_{m5}\frac{v_{id}}{2} + g_{m6}\frac{v_{id}}{2} \\ &= \frac{1}{2}v_{id}(g_{m5} + g_{m6}) \\ \rightarrow G_m &= \frac{1}{2}(g_{m5} + g_{m6}) \end{aligned}$$

Output resistance

To find the output resistance, all independent sources are shorted and a test voltage is attached to the output as shown in Figure 4.5.

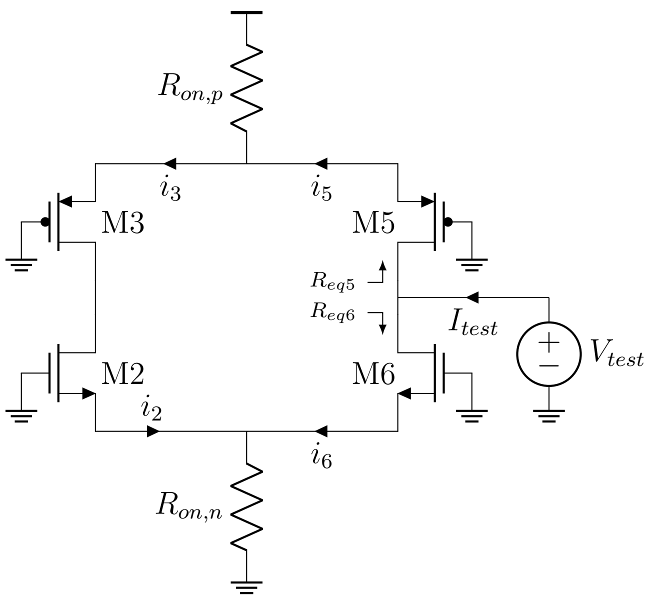

Figure 4.5: Schematic for R_{out} calculation.

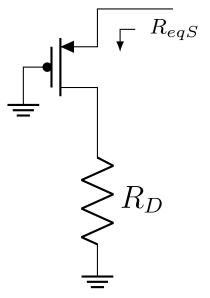

(a) Looking into the source

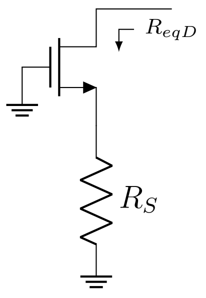

(b) Looking into the drain

Figure 4.6: Equivalent MOSFET resistances.

The equivalent resistances in Figure 4.6 are $R_{eqS} = \frac{r_o+R_D}{g_m r_o+1}$ (4.6a) and $R_{eqD} = r_o + g_m r_o R_S$

(4.6b). These equivalences are used to solve for the output resistance of the TIA.

$$
\begin{aligned}
R_{out} &= \frac{V_{test}}{I_{test}} \\
I_{test} &= i_5 + i_6 = \frac{V_{test}}{R_{eq5}} + \frac{V_{test}}{R_{eq6}} \\
R_{eq5} &= r_{o5} + g_{m5} r_{o5} \cdot (R_{on,p} || R_{eqS,3}) \\
&= r_{o5} + g_{m5} r_{o5} \cdot \left(R_{on,p} \; \Big|\Big| \; \frac{r_{o3} + g_{m2} r_{o2} R_{on,n}}{g_m r_{o3} + 1} \right) \\
&\approx r_{o5} + g_{m5} r_{o5} \cdot \left(R_{on,p} \; \Big|\Big| \; \frac{1}{g_m} + R_{on,n} \right) && (g_m r_o \gg 1)
\end{aligned}
$$

The transconductance g_m of a MOSFET in saturation is defined as

$$
g_m = \left. \frac{\delta I_{DS}}{\delta V_{GS}} \right|_{V_{DS}} = \mu C_{ox} \frac{W}{L} (|V_{GS}| - |V_T|)
$$

and the on resistance of a MOSFET in triode is

$$
R_{on} = \left. \frac{\delta V_{DS}}{\delta I_{DS}} \right|_{V_{GS}} = \frac{1}{\mu C_{ox} \frac{W}{L} (|V_{GS}| - |V_T|)}
$$

assuming the square law model for a MOSFET. It can therefore be assumed that R_{on} and $\frac{1}{g_m}$ are of similar magnitude and $R_{on} \ll R_{on} + \frac{1}{g_m}$. Therefore,

$$
\begin{aligned}
R_{eq5} &\approx r_{o5}(1 + g_{m5} R_{on,p}) \\
R_{eq6} &\approx r_{o6}(1 + g_{m6} R_{on,n}) && \text{(symmetry)} \\
R_{out} &= r_{o5}(1 + g_{m5} R_{on,p}) || r_{o6}(1 + g_{m6} R_{on,n}) \\
&= \frac{1}{2} r_o (1 + g_m R_{on})
\end{aligned}
$$

Therefore, the voltage gain is $A_V = (g_{m1} + g_{m2}) \left(r_{o5}(1 + g_{m5} R_{on,p}) || r_{o6}(1 + g_{m6} R_{on,n}) \right)$ and the TIA gain is

$$
\begin{aligned}
\frac{V_{\text{out}}}{I_{\text{in}}} &\approx - \frac{2 g_m \cdot \frac{1}{2} r_o (1 + g_m R_{on})}{1 + 2 g_m \cdot \frac{1}{2} r_o (1 + g_m R_{on})} R_f \\
&= - \frac{g_m r_o (1 + g_m R_{on})}{1 + g_m r_o (1 + g_m R_{on})} R_f
\end{aligned}
$$

Noise analysis

To calculate the noise current variance at the TIA output, the individual contributions from each equivalent noise generator shown in Figure 4.7 is considered using superposition.

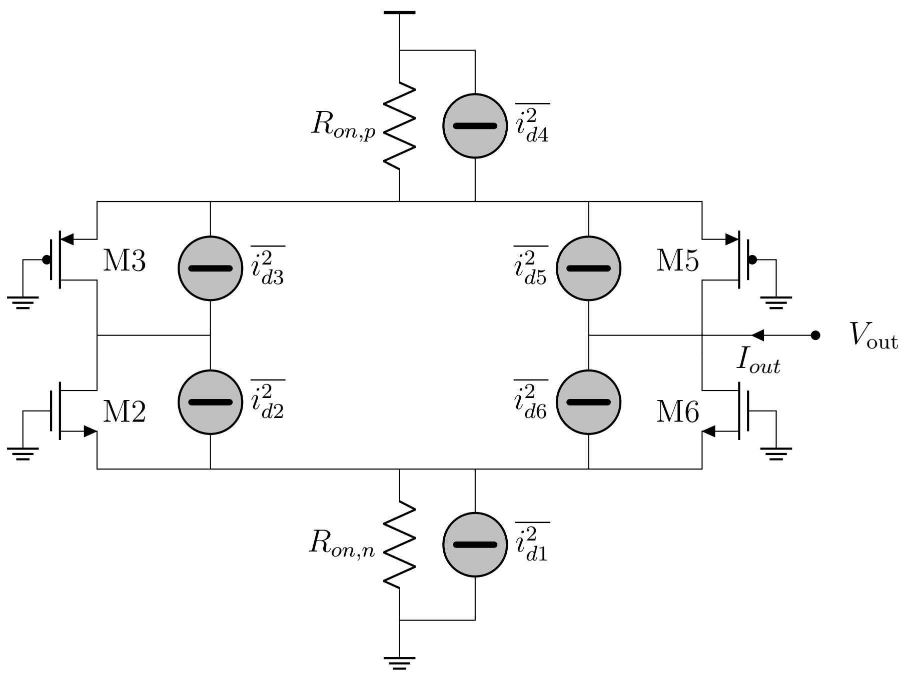

Figure 4.7: Schematic of proposed AFE implementation with equivalent noise generators, where $\overline{i_{dk}^2} = 4kT\gamma g_{mk}\Delta f$.

Intuitively, it can be seen in Figure 4.7 that this circuit has twice the number of noise sources due to the two branches of the circuit in addition to the noise contributions from the tail transistors. Therefore, the noise spectral density at the output is expected to be significantly larger than that of the current TIA implementation ($2kT\gamma g_m r_o^2 \Delta f$, calculated in Section 4.1). This will be verified in simulation in Section 4.3.

Comparison of the two topologies

Both topologies utilize current reuse and are able to leverage the transconductance of both the NMOS and PMOS inputs. The proposed TIA has a differential input, which allows for common mode noise cancellation. However, the output noise spectral density of the proposed topology is significantly larger than noise of the current topology. The proposed topology has a higher voltage gain due to its larger output resistance, so its TIA gain is closer to $-R_f$ as desired.

The tail NMOS and PMOS transistors limit the output voltage headroom, but since they can be operated in triode, the drain voltage can be close to the rail [1] and headroom is not affected significantly.

As the proposed topology has 4 more transistors than the current topology, each AFE will take up a larger area. Assuming the complementary transistors (M2, M3, M5, and M6) in the proposed topology have the same $g_m = \frac{2I_D}{V^*}$ as the input pair in the current topology, the proposed topology would require twice as much current as the existing TIA due to its differential nature. However, the larger area and higher power consumption do not matter too much, as the AFE is remoted outside of the body where size and power consumption are less of a constraint.

The bias voltage in the proposed topology enables greater user control over the tail current and power consumption. Furthermore, the self-biased tail transistor M1 eliminates the need for a complex common mode feedback loop [3]. If the common mode input voltage range is limited, M4 can be self-biased as well by connecting its gate to the drains of M2 and M3 [1].

4.3 Simulation Results

Simulations were run to verify the gain and noise analyses from the previous section and help compare the relative performance of the two topologies.

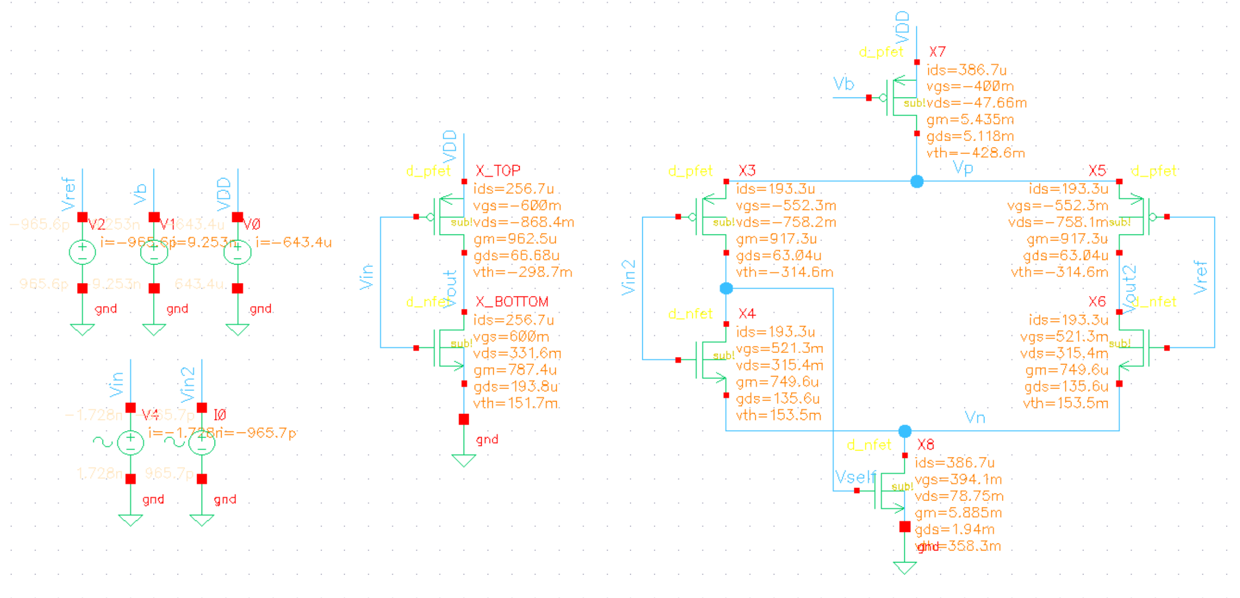

Figure 4.8: Schematic of testbench with both TIA implementations (including DC operating points) with feedback resistor omitted.

Figure 4.8 includes a schematic of the testbench for both topologies. The noise contribution of the feedback resistor was neglected. The transistors were sized such that g_{mp} and r_{op} for the PMOS transistors in each complementary pair are the same and g_{mn} and r_{on} for the NMOS transistors in each complementary pair are the same across both circuits. The tail NMOS at the bottom was sized with twice the width of the complementary NMOS transistors and the tail PMOS at the top was sized with twice the width of the complementary PMOS transistors. The following parameters were used: $V_{DD} = 1.2$V, $V_b = 0.8$V, $V_{ref} = 0.6$V, and $f = 30$MHz, where f is the frequency of the sinusoidal voltage input.

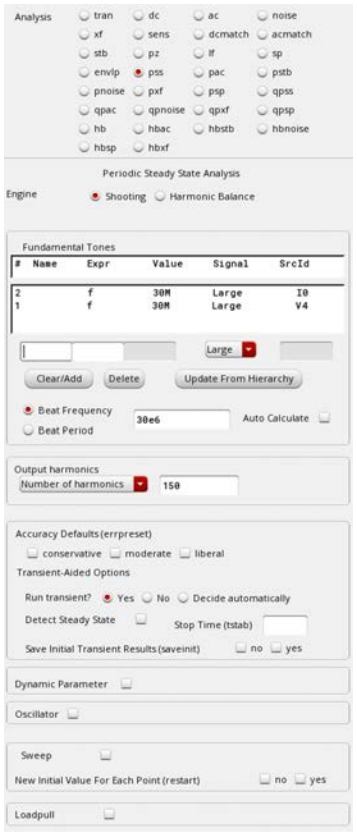

Analysis: [✓ pss]

Periodic Steady State Analysis

Engine: [✓ Shooting] Harmonic Balance

Fundamental Tones

#	Name	Expr	Value	Signal	SrcId
2		f	30M	Large	I0
1		f	30M	Large	V4

[✓ Beat Frequency] Beat Period: 30e6 Auto Calculate ☐

Output harmonics: Number of harmonics 150

Accuracy Defaults (errpreset): ☐ conservative ☐ moderate ☐ liberal

Transient-Aided Options

Run transient? [✓ Yes] No Decide automatically

Detect Steady State ☐ Stop Time (tstab)

Save Initial Transient Results (saveinit) ☐ no ☐ yes

Dynamic Parameter ☐

Oscillator ☐

Sweep ☐

New Initial Value For Each Point (restart) ☐ no ☐ yes

Loadpull ☐

(a) PSS simulation setup.

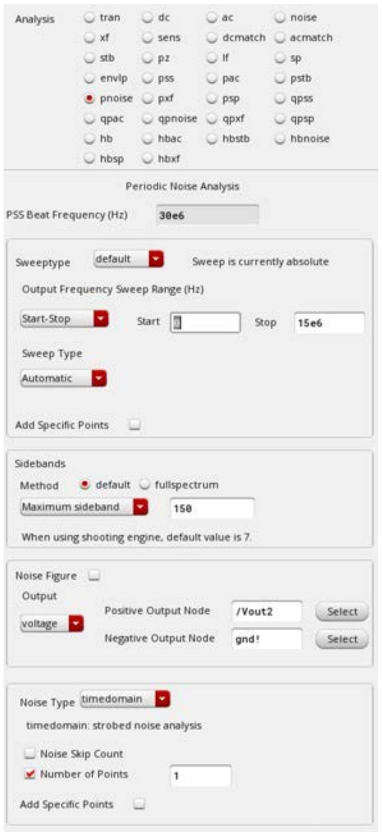

Analysis: [✓ pnoise]

Periodic Noise Analysis

PSS Beat Frequency (Hz): 30e6

Sweeptype: default — Sweep is currently absolute

Output Frequency Sweep Range (Hz): Start-Stop, Start 1, Stop 15e6

Sweep Type: Automatic

Add Specific Points ☐

Sidebands

Method: [✓ default] fullspectrum

Maximum sideband: 150

When using shooting engine, default value is 7.

Noise Figure ☐

Output: voltage

Positive Output Node: /Vout2

Negative Output Node: gnd!

Noise Type: timedomain

timedomain: strobed noise analysis

☐ Noise Skip Count

✓ Number of Points: 1

Add Specific Points ☐

(b) PNOISE simulation setup

Figure 4.9: Noise simulation setup.

Figure 4.9 displays the simulation setup for the noise analysis. A periodic steady state (PSS) simulation is run first to determine the periodic operating point and a PNOISE simulation is run subsequently to calculate the total noise.

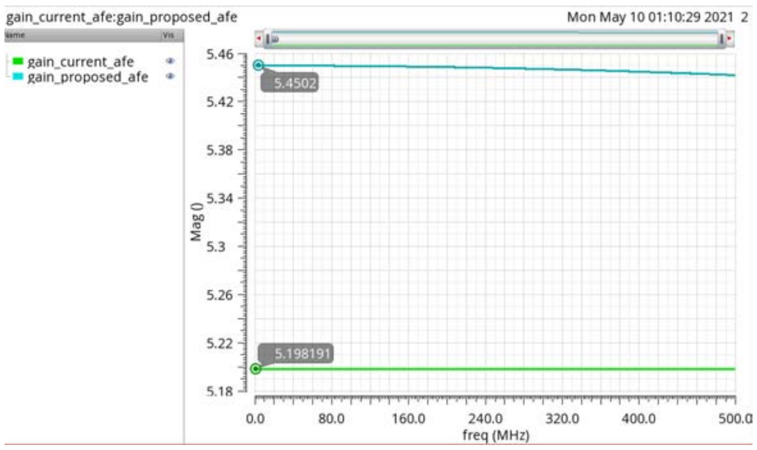

Figure 4.10: Voltage gain A_V of each TIA implementation.

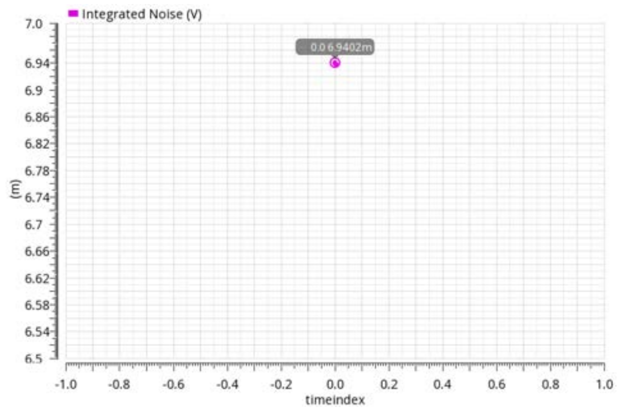

(a) Integrated noise for current topology (V).

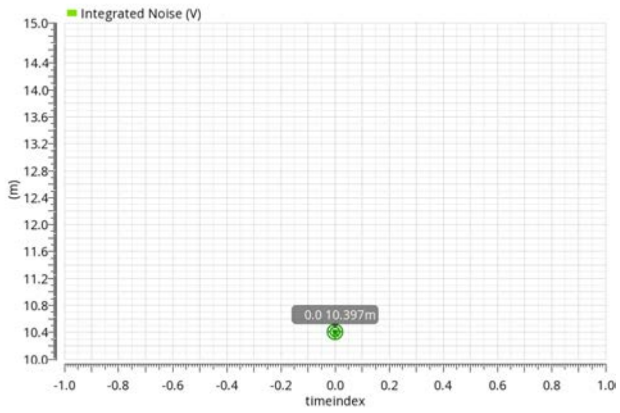

(b) Integrated noise for proposed topology (V).

Figure 4.11: Noise simulation results.

As shown in 4.10, the voltage gain of the proposed TIA (≈ 5.45) is slightly higher than the gain of the existing TIA (≈ 5.2). This aligns with the calculations in Sections 4.1 and 4.2:

$$\frac{A_{V,\text{proposed}}}{A_{V,\text{current}}} = 1 + g_m R_{on} > 1$$

Figure 4.11 displays the integrated noise at the output for each TIA topology. As expected, the noise at the output of the proposed topology (10.397 mV) is significantly higher than the noise at the output of the current topology (6.9402 mV) by a factor of about 1.5.

Chapter 5

Conclusion and Future Work

Silicon MRRs are a promising alternative to established PMUT and CMUT based ultrasound imaging systems. By demonstrating proof of concept through measurement results and optimizing both the photonic layout and circuit design of the system, MRR-based ultrasound imaging presents a solution for the disadvantages of commercial systems.

An important next step in testing the current prototype chip is to transition to processing data in real-time on an FPGA as well as implement beamforming in order to generate real-time images (as opposed to using the script detailed in Figure 2.9). In terms of photonic layout, implementing a smaller size, lower power frontend for the sensing rings will help accommodate a 50 μm pitch between the MRRs and thus enable the layout demonstrated in Chapter 3. Furthermore, as the topology proposed in Chapter 4 does not appear significantly advantageous over the current inverter-based TIA due to its greater thermal noise, it is worth exploring alternate TIA implementations.

Bibliography

[1] M. Bazes. “Two novel fully complementary self-biased CMOS differential amplifiers”. In: *IEEE Journal of Solid-State Circuits* 26.2 (1991), pp. 165–168. DOI: `10.1109/4.68134`.

[2] Man-Chia Chen et al. “A Pixel Pitch-Matched Ultrasound Receiver for 3-D Photoacoustic Imaging With Integrated Delta-Sigma Beamformer in 28-nm UTBB FD-SOI”. In: *IEEE Journal of Solid-State Circuits* 52.11 (2017), pp. 2843–2856. DOI: `10.1109/JSSC.2017.2749425`.

[3] Michele D’Urbino et al. “An Element-Matched Electromechanical $\Delta\Sigma$ ADC for Ultrasound Imaging”. In: *IEEE Journal of Solid-State Circuits* 53.10 (2018), pp. 2795–2805. DOI: `10.1109/JSSC.2018.2859961`.

[4] V. I. Kopp et al. “Chiral Fibers: Microformed Optical Waveguides for Polarization Control, Sensing, Coupling, Amplification, and Switching”. In: *Journal of Lightwave Technology* 32.4 (2014), pp. 605–613. DOI: `10.1109/JLT.2013.2283495`.

[5] Jing Li et al. “A 1.54mW/Element 150μm-Pitch-Matched Receiver ASIC with Element-Level SAR/Shared-Single-Slope Hybrid ADCs for Miniature 3D Ultrasound Probes”. In: *2019 Symposium on VLSI Circuits*. 2019, pp. C220–C221. DOI: `10.23919/VLSIC.2019.8778200`.

[6] Wouter J. Westerveld et al. “Opto-Mechanical Ultrasound Sensor Based on Sensitive Silicon-Photonic Split Rib-Type Waveguide”. In: *2019 Conference on Lasers and Electro-Optics Europe/European Quantum Electronics Conference*. 2019. DOI: `10.1109/CLEOE-EQEC.2019.8873214`.

[7] Panagiotis Zarkos, Olivia Hsu, and Vladimir Stojanović. “Ring Resonator Based Ultrasound Detection in a Zero-Change Advanced CMOS-SOI Process”. In: *Conference on Lasers and Electro-Optics*. Optical Society of America, 2019, JW2A.78. DOI: `10.1364/CLEO_AT.2019.JW2A.78`. URL: `http://www.osapublishing.org/abstract.cfm?URI=CLEO_AT-2019-JW2A.78`.

[8] Panagiotis Zarkos et al. “Monolithically Integrated Electronic-Photonic Ultrasound Receiver Using Microring Resonator”. In: *Conference on Lasers and Electro-Optics*. (in press). Optical Society of America.